Construction and Building Materials 401 (2023) 132906

Contents lists available at ScienceDirect

Construction and Building Materials

journal homepage: www.elsevier.com/locate/conbuildmat

Feasibility of iron-based shape memory alloy strips for shear strengthening of damaged RC beams promoting the formation of plastic hinges

Celia Traver [a], Joaquín G. Ruiz-Pinilla [b,*], Andrea Monserrrat [a], Luis A. Montoya-Coronado [b], Pedro F. Miguel [a], Carlos Ribas [b], Antoni Cladera [b], José L. Bonet [a]

[a] ICITECH, Universitat Politècnica de València, Valencia 46022, Spain
[b] Department of Industrial Engineering and Construction, University of the Balearic Islands, Palma 07122, Spain

ARTICLE INFO

Keywords:
Iron-based shape memory alloy
Shear strength
Damaged reinforced concrete beams
Plastic hinge
External strips
Cantilever beam
Continuous beam
Rotation capacity
Prestressing
Experimental study

ABSTRACT

This research focuses on the proof of concept of the feasibility of iron-based shape memory alloys strips (Fe-SMA) to strengthen damaged structures by promoting the yielding of longitudinal reinforcement. For this purpose, an experimental campaign on real-scale reinforced concrete beams previously damaged on shear and retested after being strengthened was carried out. The strengthening technique consists of external Fe-SMA strips wrapping the beams. The results show a very significant increase in both shear strength and ductility. In addition, shear predictions were calculated and compared by several design models. This study highlights the potentialities of Fe-SMA as a strengthening technique for damaged beams on shear.

1. Introduction

Interest in extending the safety and lifetime of existing structures has grown in the construction industry, magnified by a significant drop in government investment in new infrastructure. Unfortunately, the materials used to build our structures do not permanently conserve their properties and progressive ageing causes them to deteriorate. This fact has promoted the development of new technologies to repair and strengthen reinforced concrete (RC) elements. Some of these technologies focus on the shear strengthening of beams because this failure is associated with feared sudden collapses.

Shear behaviour is continuously being investigated by many research groups [1–6]. However, the shear models of code/standards approaches have been discussed for decades and still have some compatible conceptual differences with the complex redistribution of internal stresses at failure [7]. Nothing has been settled for design codes about how to consider shear strength provided by concrete and stirrups for RC elements. ACI CODE 318-19 [8], Model Code 2010 [9] and CSA A23.3-14 [10] include concrete and steel terms. However, Eurocode 2 [11] considers only one term, in which concrete contribution is accounted for by modifying the steel contribution by inclining the compression field.

Several retrofitting systems have been used with different techniques and materials. Traditional systems include the use of fibre-reinforced polymer (FRP) sheets/plates and aluminium or steel plates [12–15]. In addition, recent studies have been conducted to investigate fibre-reinforced cementitious matrix (FRCM) composites [16,17] or hybrid strengthening materials [18,19]. Nevertheless, in most current technologies, strengthening materials start working after increasing external loads. Therefore, the deformation of a strengthened structure up to a certain level of damage is needed before the strengthening material begins to contribute. However, shape memory alloys (SMA) can introduce prestressing forces on elements from the time they are installed, and can be activated without using complex or expensive auxiliary devices. Accordingly, interest in using SMA has grown in recent years. Recent research into the use of iron-based shape memory alloys (Fe-SMA) proves its advantages for use in civil engineering structures [20–33]. Nonetheless, these research works are still ongoing and more studies are necessary.

Prestressing force is possible owing to the material's Shape Memory Effect (SME). This characteristic allows a prestrained SMA to revert to its original shape upon heating and cooling (activation). By restraining the deformation recovery while activating, tensile stress is generated in SMA, which results in a prestressing force for the underlying structure

* Corresponding author.
E-mail address: joaquin.ruiz@uib.es (J.G. Ruiz-Pinilla).

https://doi.org/10.1016/j.conbuildmat.2023.132906
Received 28 May 2023; Received in revised form 12 July 2023; Accepted 7 August 2023
Available online 13 August 2023

Notation

a	shear span (defined as $M_{1,R}/V_{R,test} + d/2$)
A_{strip}	area of external Fe-SMA strips considering two branches per strip
d	effective depth
E_c	modulus of elasticity of concrete
$E_c(t)$	modulus of elasticity of concrete at t days
E_s	modulus of elasticity of reinforcement
f_c	cylinder concrete compressive strength
$f_c(t)$	cylinder concrete compressive strength at t days
f_{ct}	concrete tensile strength
f_u	reinforcement tensile strength
f_y	reinforcement yield stress
$f_{sw,u}$	shear reinforcement tensile strength
$f_{sw,y}$	shear reinforcement yield stress
l_i	cantilever length ($i = 1,3$) or span ($i = 2$)
l_j	segment of span ($j = a,b,c$)
$M_{1,R}$	absolute value of bending moment at failure (at $d/2$ from the section of support A in cantilever tests and from section of support B in the span test)
$M_{2,R}$	bending moment at failure (at $d/2$ from the section of applied P_2 in the span test)
M_y	bending moment when flexural reinforcement is yielded
P_i	applied load ($i = 1,2$)
$P_{i,R}$	applied load ($i = 1,2$) at failure
R_A	reaction in support section A
R_B	reaction in support section B
V	shear force
V_c	shear strength provided by concrete
$V_{c,test}^{k}$	range of shear strength provided by concrete in tests ($k = inf, sup$)
$V_c^{confinement}$	increase in concrete contribution due to confinement by external shear reinforcement
V_{Rd}	predicted shear strength by design code
$V_{R,test}$	shear strength in tests, including self-weight
V_s	shear strength provided by shear reinforcement
$V_{s,test}$	shear strength provided by shear reinforcement in tests
V_{SMA}	shear strength provided by external Fe-SMA strips
$V_{SMA,test}^{k}$	range of shear strength provided by external Fe-SMA strips in tests, considering free recovery strain ($k = inf$) or constrained recovery strain ($k = sup$)
V_y	shear force corresponding to the full flexural strength of beams
Δv_{cu}	non-dimensional confinement factor
δ_i	beam deflection under applied load ($i = 1,2$)
$\varepsilon_{sw,0}$	shear reinforcement strain at the end of the original tests (B12C, B15C and B15S)
$\varepsilon_{sw,u}$	shear reinforcement strain at maximum load
$\varepsilon_{sw,y}$	yield strain of shear reinforcement
ε_u	reinforcement strain at maximum load
θ	angle between principal web compression due to shear and the axis of the member
θ_B	slope at support B in span tests
$\theta_{B,I}$	slope at support B at the end of the first phase in span tests
ρ	tensile reinforcement ratio
ρ_w	shear reinforcement ratio
$\varnothing$	reinforcing bar nominal diameter
σ_{SMA}^{k}	range of tensile stress of external Fe-SMA considering free recovery strain ($k = inf$) or constrained recovery strain ($k = sup$)
σ_{sw}	shear reinforcement tensile stress
ψ_b	bending rotation of beams, or increase of bending rotation in strengthened tests
$\psi_{b,f}$	bending rotation of beams at the end of the test or increase of bending rotation in strengthened tests
$\psi_{b,R}$	bending rotation of beams at failure or increase in the bending rotation in strengthened tests
w_{mean}	mean of critical shear crack width or mean increase in the CSC width in strengthened tests
$w_{mean,f}$	mean of critical shear crack width at the end of the test or mean increase in the CSC width in strengthened tests
$w_{mean,R}$	mean of critical shear crack width at failure or mean increase in the CSC width in strengthened tests

[25,34], which is called recovery stress. This property is the result of the martensitic transformation, which is a reversible phase transformation [35].

Montoya-Coronado et al. [34] studied the feasibility of strengthening beams testing on shear using Fe-SMA. Strengthening of beams was done by Fe-SMA strips applied to small-scale RC beams. That research work displayed the increased shear strength and ductility of beams by validating a new anchorage system for Fe-SMA strips using full-wrapping. Ruiz-Pinilla et al. [36] performed an FE analysis of this experimental campaign by implementing newly proposed analytical stress–strain curves of Fe-SMA based on the modified Ramberg-Osgood models for non-linear materials [37]. The parameters of the stress–strain equations have been adjusted from a large number of tensile tests. The results concluded that the appearance of shear cracks was delayed on the specimens in which the activation of strips took place. Similar results were found by Shahverdi et al. [38], who used ribbed stirrups (Fe-SMA ribbed bars) combined with shotcrete mortar. The authors concluded that prestressing was the cause of smaller crack widths for service loads. Zerbe et al. [19] and Cladera et al. [39] carried out experimental campaigns with Fe-SMA strips, used as shear external strengthening on RC beams with a T cross-section. They showed that shear strength increased, but the results were negatively conditioned by the influence of the anchorage system.

Most experimental campaigns have studied the shear behaviour of RC-strengthened beams by running tests performed on simply supported beams. Nevertheless, the bending moment-shear strength interaction is a distinctive feature of continuous beams. In these situations, potential shear failure regions are simultaneously subjected to maximum shear forces and bending moments. The formation of plastic hinges with marked rotations enables the redistribution of bending moments before developing full structural strength [40]. Therefore, plastic hinges of continuous beams must resist large shear forces while developing considerable rotations, which may cause shear strength to reduce in these critical plastic zones [40–43]. This interaction may be particularly relevant to statically indeterminate structures, which may fail in shear after yielding of flexural reinforcement and with increasing shear forces in critical plastic regions.

This paper presents an experimental shear strength study that involves the strengthening with external Fe-SMA strips of two previously tested continuous RC beams until failure [40,41]. The experimental programme was developed at the Institute of Concrete Science and Technology (ICITECH) of the Universitat Politècnica de València (UPV,

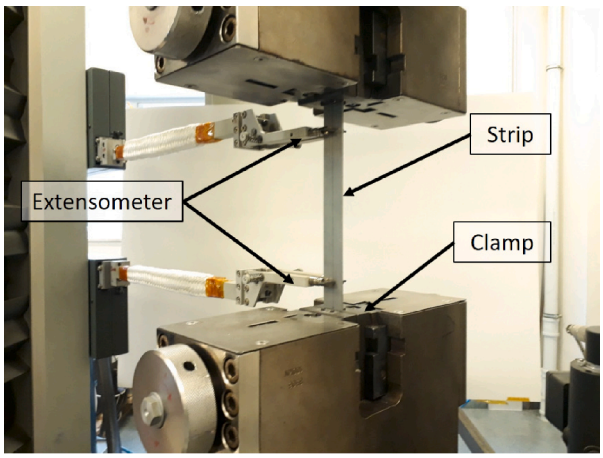

Fig. 1. A 300 mm free-length Fe-SMA strip installed in a Zwick Z100 universal testing machine equipped with an extensometer over a length of 250 mm.

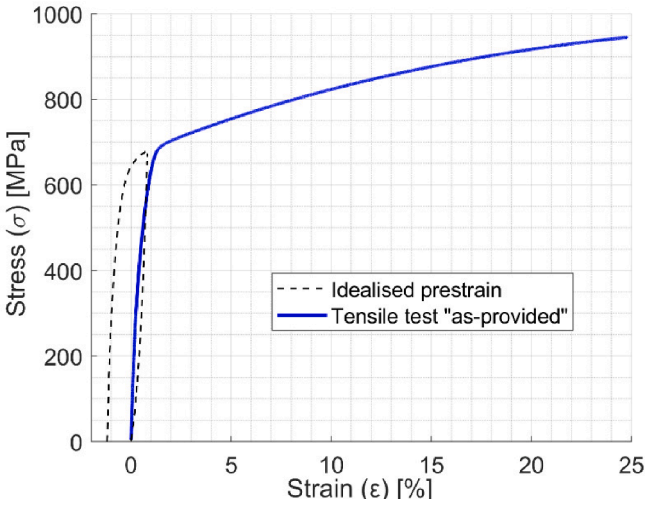

Fig. 2. Stress–strain curve of the as-provided Fe-SMA by the manufacturer.

Spain). Three tests were carried out on those two different reused beams. Beams were real-scale elements and presented significant damage upon shear (the initial tests were stopped after beams' failure). The main objective was to study the feasibility of applying Fe-SMA strips to critical shear specimens to return to the initial degree of safety, improving their ductility if possible. An identical Fe-SMA material has been used in the previous experimental campaign by the authors on RC beams with a T cross-section [39], but with another anchorage system due to the different shape of beams' cross-section. Instead during the current campaign, beams had a rectangular cross-section, and strips were wrapped around the beam and anchored to themselves. An innovative test setup previously developed by the authors has been used [40,41]. This test procedure allows the shear response of cantilever beams (statically determinate structures) and of the plastic-hinge zones in continuous beams failing in shear to be analysed after yielding flexural reinforcement and redistributing internal forces (statically indeterminate structures). Moreover, this paper includes a comparison of the shear strength predictions of the strengthened beams by several existing shear procedures: Model Code 2010, ACI CODE-318–19) [8], Eurocode 2 [11] and the Compression Chord Capacity Model.

2. Fe-SMA strips characterisation

Fe-SMA strips were provided by the manufacturer in the form of a coil that was 120 mm wide and 1.5 mm thick, prestrained at 2% of its original length. The manufacturing process and the detailed production procedure of the Fe-SMA material and strips are described in [29]. The recommendations for the characterisation of the test setup and protocols are detailed in [23]. A previous characterisation of 0.5 mm-thick Fe-SMA similar strips is presented in [34]. The original strips were cut into narrower 25 mm-width strips for characterisation purposes by employing a water jet cutting process (the same width was used for characterisation in reference [34]), and into 30 mm-width strips to use them as external strengthening for the tested beams. To obtain this material's mechanical properties, several tests were run in a Z100 Zwick universal tensile machine with a 100 kN load cell. Then 30 mm-width samples were tested with a free length equalling 300 mm and 15 mm inside each clamp to grip the sample to avoid slipping. Fig. 1 shows a tensile test with an extensometer base length that equals 250 mm.

2.1. Mechanical properties

The ultimate strength of the "as-provided" Fe-SMA strips approximately equalled 940 MPa with 25% ultimate strain. Ultimate strength was similar to that provided in previous research works [29]. Nevertheless, ductility was lower, as previous research works have signalled failure strains exceeding 40%. This ultimate strength reduction could be caused by some imperfections produced while cutting the strips. However, this was not investigated because 25% of the strain was satisfactory for the envisaged application.

A typical stress–strain curve is presented in Fig. 2. Note that for stress of approximately 690 MPa, the curve shows a very marked change in behaviour related to the previous prestraining process (on the discontinuous black line) carried out by the manufacturer. The black dotted lines in Fig. 2 and Fig. 3a have been approximated by the results of the prestraining processes published in [29]. For the "as- provided" Fe-SMA strip, the mean modulus of elasticity measured during the tensile test (the blue line in Fig. 2) within a stress range of 20–200 MPa was around 144 GPa, and a lower value (111 GPa) was obtained by computing between 100 and 300 MPa. The mean 0.2% proof stress, obtained by the off-set method using the first presented modulus of elasticity, came close to 470 MPa.

Activation of Fe-SMA strips can result in the generation of recovery stresses, provided there is no gap between strip and beam surface. However, if excessive gaps exist, Fe-SMA will exhibit free-recovery strain without generating prestressing forces. Consequently, the recovery stress and free recovery shape would represent distinct states for Fe-SMA, as further detailed in the following section.

2.2. Recovery stresses and free-recovery shape

To obtain recovery stress, an as-provided Fe-SMA strip was placed in the universal testing machine and an initial prestress of 40 MPa was applied. Then the strip was heated up to approximately 160 °C using a heat gun before being left to cool down (Fig. 3b). During the heating and cooling process, sample deformation was prevented by forcing the strain measured by the extensometer staying constant (see Fig. 1). As the sample tended to shorten due to reverse martensitic transformation due to the heating and cooking process in an attempt to recover the initial "shape" (that before prestraining), the tensile stress in the sample rose to above 349 MPa (see Fig. 3b). This recovery stresses value is completely compatible with the recovery stresses reported in [29]. The complete temperature-recovery stress curves for similar strips are presented in [29,34]. After generating recovery stresses, the tangent modulus of elasticity was 32.2 GPa when measured within the 400–500 MPa range. By the 0.2% off-set method, a 0.2% proof stress of 626 MPa was calculated in this state. In the presence of a free-recovery shape (as depicted

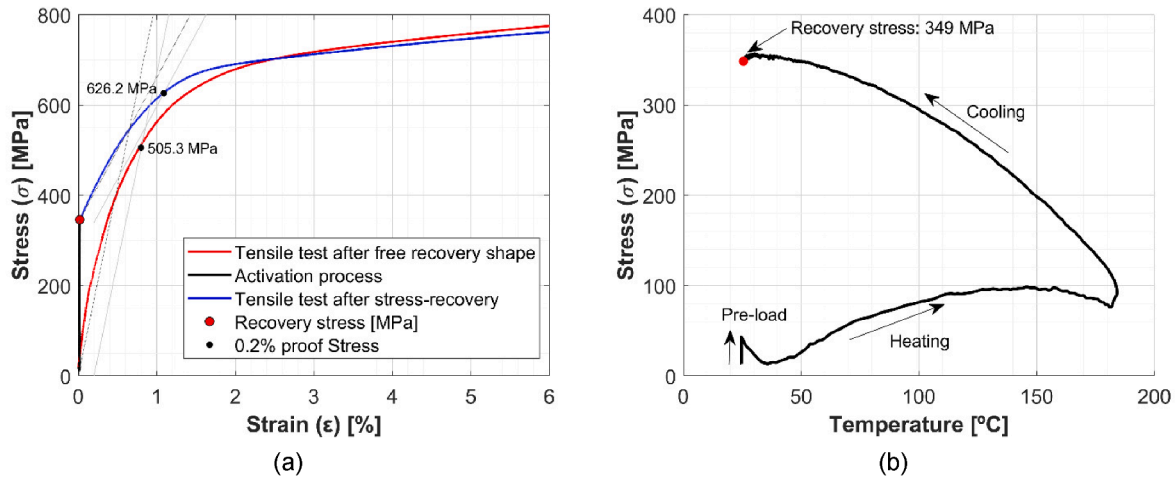

Fig. 3. Recovery stress and the final monotonic test: (a) experimental stress–strain curve for the activated Fe-SMA strip with 100% and 0% recovery stress situations; (b) recovery stress–temperature test.

by the red curve in Fig. 3a), the tangent modulus of elasticity was 83.9 GPa within the 100–300 MPa range. The corresponding 0.2% proof stress was, in this case, determined to be 505 MPa.

3. Description of the experimental program

During this experimental campaign, two previously tested continuous reinforced concrete beams (specimens B12 and B15) were strengthened and retested. Both specimens were 7.00 m long with rectangular cross-sections that were 250 mm wide and 450 mm high. The scheme of the geometry, reinforcement and load configuration, which is described below, is shown in Fig. 4. These two specimens were chosen from a previous experimental programme that analysed the shear strength of cantilever and continuous RC beams according to different shear reinforcement ratios [41]. The chosen specimens were very interesting in that experimental campaign according to the initial behaviour and level of damage. The specimens' initial cracking pattern is exhibited in Fig. 4 for the studied zones. The strengthening of the beams was designed to show the feasibility of using external Fe-SMA strips to strengthen shear critical RC beams. As this research was done as a proof test, further research by varying different parameters should be carried out to study its influence on both shear strength and rotation capacity.

Beams were tested according to two different load configurations to obtain shear failures in both statically determinate and indeterminate structures. Three shear tests were carried out on these two beams: two cantilever tests (CE) and one continuous beam test (SE). Beam B12 was tested in the CE test configuration, and beam B15 in both test configurations CE and SE.

The main objective when designing the specimens for the previous experimental campaign [41] was to allow shear failures with different rotation levels to be developed within a wide range of values, and before or after plastic hinge formation. Thus it was possible to study how the development of rotations, related to flexural behaviour, governs shear strength in RC specimens with shear reinforcement, including those shear failures developed after yielding of the longitudinal reinforcement.

A code with four terms was used in [41] to label each test conducted on specimens B12C-R0-S3-L1, B15C-R2-S3-L1 and B15S-R2-S3-L4. The first term denoted the tested beam and the type of test (*C* -by cantilever- for the CE test and *S* -by span- for the SE test). The second term represented the specimen series according to shear reinforcement. R0 (without shear reinforcement) and R2 ($\rho_w = 0.20\%$, two-legged closed stirrups Ø8 spaced at 200 mm along the critical zones where shear failure was expected), respectively for specimens B12 and B15 (see Fig. 4). In addition, to prevent shear failure outside the expected failure regions, stirrups were provided in those zones with a reinforcement ratio of 0.90% (stirrups Ø12 spaced at 100 mm) in both specimens. The third term represented the specimen section according to the longitudinal steel reinforcement (S1, S2 or S3). Both specimens B12 and B15 had the same longitudinal reinforcement, S3 ($\rho = 1.94\%$, 12 Ø20 mm-diameter bars). A high reinforcement ratio was used to prevent flexural failure before shear failure in the SE tests. The effective depth *d* equalled 389 mm. The last term determines the location of load and bearing points by indicating the cantilever length in the CE tests (L1, L1.6 or L2.3) and the span length in the SE tests (L6, L5 or L4). The length of both specimens B12 and B15 was the same (L1 (1 m) in the CE test and L4 (4 m) in the SE test. After explaining the specimen designations of the initial campaign, this paper used simplified codes: B12C, B15C and B15S. The tests performed during this campaign (retrofitted specimens) were named with an R placed before their name: R-B12C, R-B15C and R-B15S.

The beams were strengthened using the Fe-SMA full wrap strips that were 1.5 mm thick and 30 mm wide. The strips helped to strengthen the beam to return and even improve the beam's initial shear capacity in the damaged area where there were shear cracks. The strengthened length corresponds approximately to the length of critical shear crack (CSC), which in CE tests matches the shear span. With the SE test, the strengthened length was 960 mm, and external plates and bars were used to strengthen the rest of the shear span without shear reinforcement to force failure in the same area as in the initial test. Four strips (strips S1 to S4) were arranged around the shear cracks from the support to the load application point (see Fig. 4). First strip S1, located next to the support, was used to confine the compression chord and to improve shear capacity. The last strip S4 ensured the dowel action of longitudinal reinforcement. The intermediate strips S2 and S3 transferred the shear load through a cracked section. In the CE tests, the separation of strips was 230 mm and 320 mm in the SE test. Note that cracks formed during the previous experimental campaign until beams' failure, which were not repaired for conducting this research (no crack injections or use of repairing mortars).

3.1. Strengthening procedure

The manufacturer previously prestrained the Fe-SMA strips to create martensite through an initial forward martensitic transformation. Therefore, the acquired material was ready to be placed on the beams. The strips fully wrapped the section of the beam anchoring to themselves by using three screws fixed with nuts and lock washers on both sides of the strips in the lap length at the top of the beam (Fig. 5).

After placing and anchoring the strips, activation was triggered by

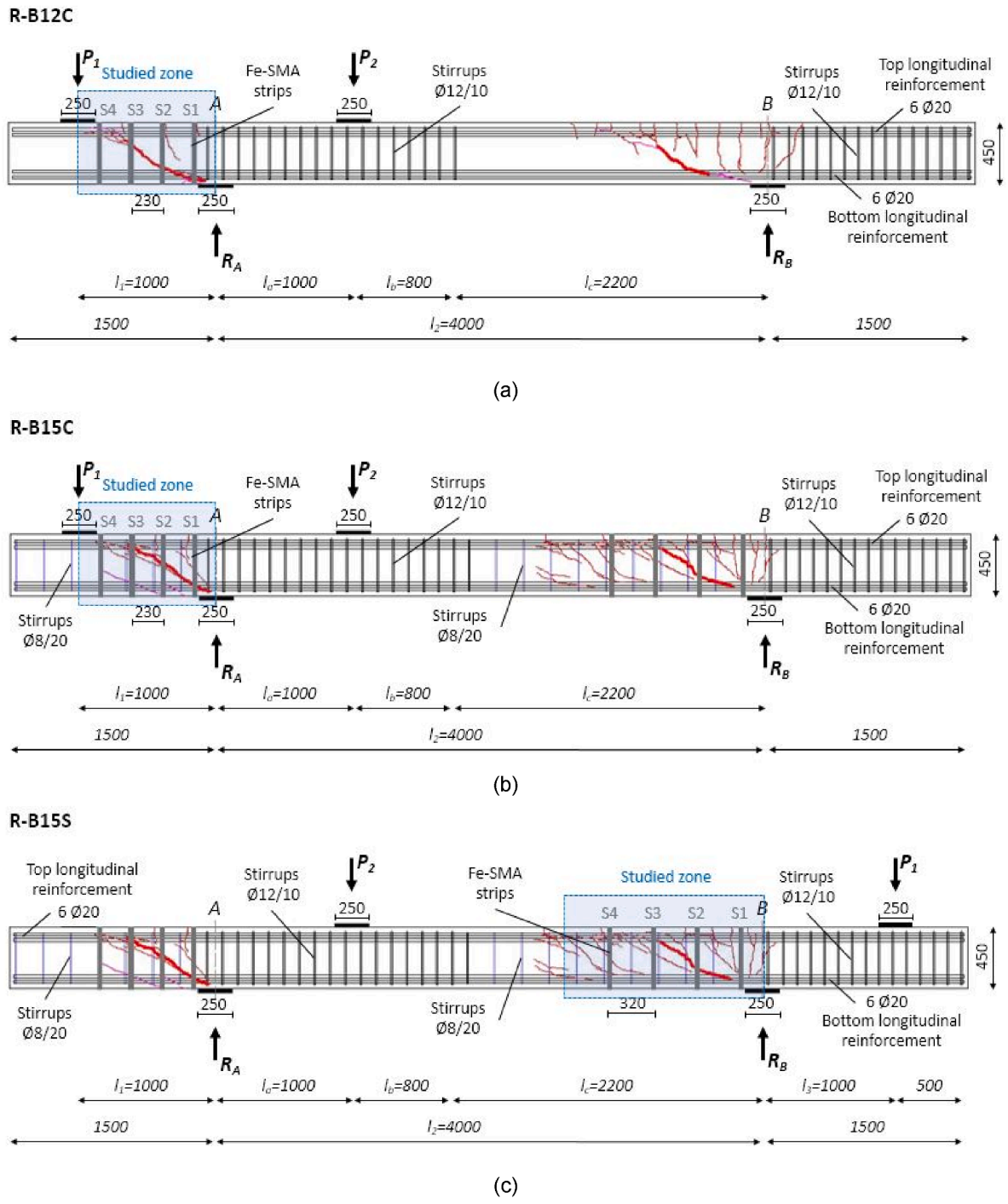

Fig. 4. Detail of the geometry, reinforcement, strengthening and load configuration of each test (dimensions in mm), adapted from [41]. The initial damage state of specimens is exhibited with the crack patterns obtained by DIC (more information is detailed in Section 4.2). (a) R-B12C; (b)R- B15C; (c) R-B15S.

producing reverse martensitic transformation from incrementing temperature with a heat gun and letting it cool down to, thus, generate recovery stresses. As the reached recovery stress value depends on the constraining of the strips, the anchorage system and the strips' good contact with the concrete surface to avoid gaps play an important role in installation [34]. Other studies by the authors [34,44] highlight the importance of avoiding gaps due to this material's relatively poor shape-recovery strain capacity. In fact, previous experimental studies have shown that the shape-recovery strain capacity of Fe-SMA is considerably low (about 1%, whereas other the shape recovery of SMA like Ni-Ti or Ni-Ti-Nb alloys lies between 6 and 8%) ([34,45]). In any case, activating Fe-SMA strips may effectively reduce small gaps after placing and anchoring the strips. In this study, when the strips were initially positioned around the beam, a slight gap existed between the surface of the beam and the strip, as shown in Fig. 6a. However, this gap was effectively eliminated following the activation process, as depicted in Fig. 6b. Nevertheless, given the difficulty of quantifying the strips' free recovery shape, the recovery stresses fall within a range between full recovery stress due to the complete strain constraint (recovery stress up to 350 MPa) and null recovery stress due to a full free recovery strain (Fig. 3a).

To avoid gaps, it was necessary to create small holes in the concrete cover and to place them inside nuts from the lower anchor system side.

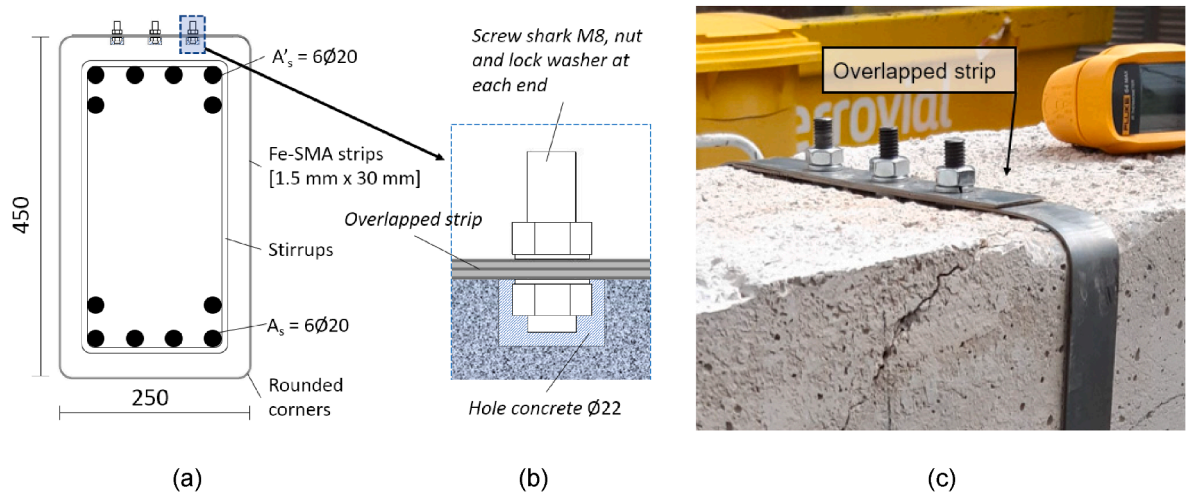

Fig. 5. Full-wrapped strengthening system. (a) cross-section of the RC beam (dimensions in mm); (b) detail of the anchoring system; (c) photography of the anchorage system.

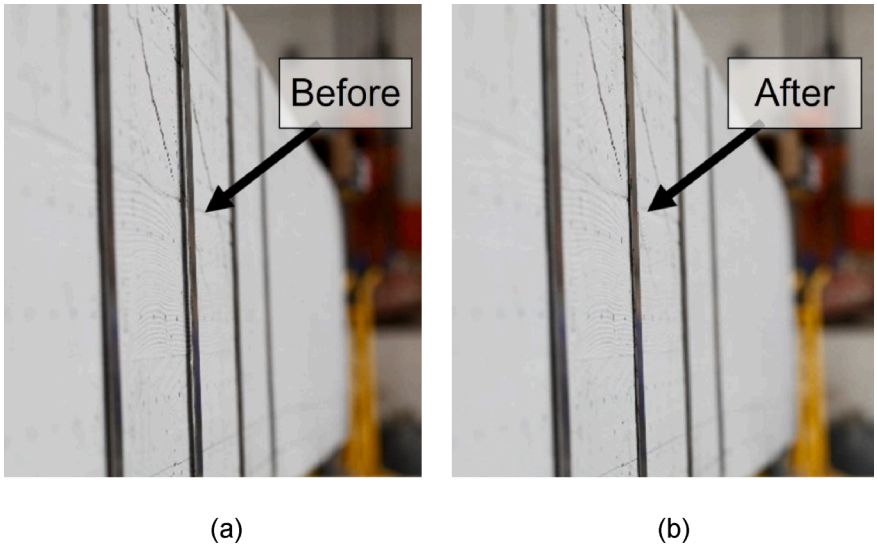

Fig. 6. Comparison before and after activating shear strengthening strips (from the photographs' perspective, the strips seem narrower than they actually are): (a) non-activated strip; (b) activated strip.

Anchorage was executed on the top of the beam where concrete is in tension due to the bending moment. This avoids affecting the compressed chord located on the downside. In real applications, holes should be filled with mortar to avoid affecting the beams' durability. Furthermore, the corners of beam sections had to be slightly rounded to reduce the concentration of stress on strips' edges and to avoid gaps as well.

The initial design of the anchorage of strips included Ø10 mm screws. However, the shear load reached during the first test (R-B12C) was higher than expected and strips failed in tension in the perforated section. Therefore, Ø8 mm screws were used for anchorage in the remaining tests (B15-specimen). Therefore, smaller holes in strips reduced the possibility of local failures. After this, no more strips failed due to holes. In contrast, one strip failed at the corner of the beam during the R-B15C test. Fig. 7 shows pictures of the two anchoring designs and the two failures of the strip of specimens R-B12C and R-B15C.

3.2. Concrete and steel properties

The mean concrete and reinforcement steel properties were obtained during the previous experimental campaign and measured as explained in [41]. The compressive strength, modulus of elasticity and tensile strength of concrete, as well as each specimen's age at the time of first testing in [41], all of which have been obtained from cylindrical specimens (diameter 150 mm and length 300 mm), are summarised in Table 1. In addition, the compressive strength and modulus of elasticity at the time of testing the strengthened beams were estimated according to Eurocode 2 [11] by taking into account the original strength, cement type and age when new tests were run. The diameter, modulus of elasticity, steel yield stress, steel tensile strength and steel strain values at the ultimate strength of longitudinal and transversal reinforcement (B500SD) are summarised in Table 2.

3.3. Test setup and procedure

The test setup was maintained from the previous experimental programme [40,41]. The beams had been subjected to two different shear tests that allowed shear failure to develop two distinct structural typologies: statically determinate structure (cantilever experiment, CE) and statically indeterminate structure (span experiment, SE). Fig. 4

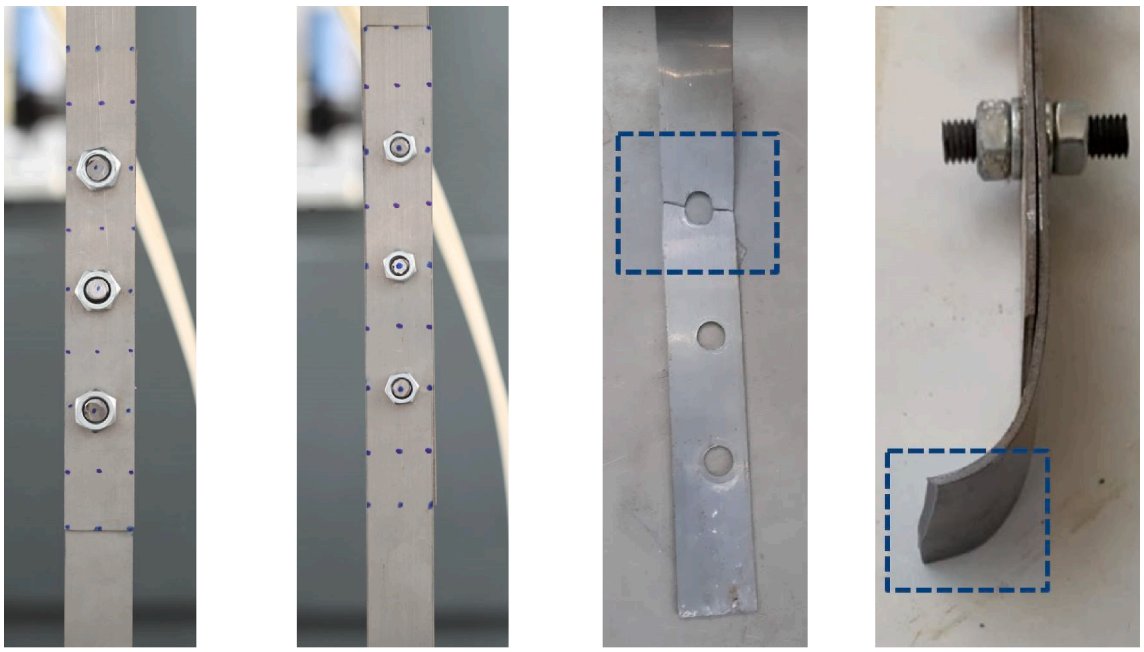

Fig. 7. Anchorage system and local failures of strips: (a) anchorage with screws Ø10 mm; (b) anchorage with screws Ø8 mm; (c) tensile failure at the perforated section of strip S3 during test R-B12C; (d) tensile failure at the corner of strips S3 during test R-B15C.

Table 1
Average values of concrete properties.

Specimen	Age upon previous testing (days)	f_c(MPa)	E_c(GPa)	f_{ct}(MPa)	Age upon testing the strengthened beams (days)	$f_c(t)$(MPa)	$E_c(t)$(GPa)
B12	22	28.7	27.5	2.9	597	36.0	29.2
B15	30	26.0	26.6	2.6	624	31.4	28.2

Table 2
Average values of longitudinal and transversal steel reinforcement.

Steel reinforcement	ϕ(mm)	E_s(GPa)	f_y(MPa)	f_u(MPa)	ε_u(%)	f_u/f_y
Longitudinal	20	206	531	639	18.3	1.20
Transversal	8	189	541	661	10.9	1.22

plots the detailed position of the applied loads and supports for both test configurations.

Loads and support reactions were transmitted to the beam through steel plates that measured 250 × 250 × 40 mm. Both the support and load systems allowed horizontal in-plane displacements and rotations, but one of the support points had restrained horizontal displacement during tests. Fig. 8 shows a diagram of the procedure for both the CE and SE tests, which is described below.

In the CE tests, load P_1 was applied by displacement control until shear failure at slow velocity (0.01 mm/s) to observe the behaviour of the beams with Fe-SMA strips. P_2 was applied by load control according to the increase in load P_1 to obtain no reaction in support B ($R_B \approx 0$). In this configuration, shear force and bending moment simultaneously increased.

The SE test was carried out in two phases. In the first phase, P_1 was applied by displacement control (0.02 mm/s) and P_2 by load control to obtain no reaction in support A ($R_A \approx 0$, a similar procedure as the CE test). During the previous experimental campaign with undamaged beams, this first phase ended when the top longitudinal reinforcement at support B yielded. In that instant, load P_1 was taken as a reference value to allow the development of the first plastic hinge in the previous tests. Thus in the current SE test (with the strengthened beam), the first phase ended when that reference value was reached. The slope of the beam at section B at the end of this phase was registered as $\theta_{B,I}$ (see Fig. 8). In the second phase, the aim was to maintain that slope constant (fixed rotation support), while the shear load at the span increased until shear failure. Therefore, P_2 was applied by displacement control (0.02 mm/s) and load P_1 by load control according to the increase in loads P_2 to maintain the slope at support B blocked. This system allows shear forces to increase at the span until second plastic hinge formation (at the section where P_2 was applied) with rising beam deflections, while the rotation on support B remained constant. Slight increases in load P_1 were necessary to maintain the slope in the second phase.

3.4. Instrumentation

Test specimens were instrumented to monitor their behaviour. The two forces applied by hydraulic jacks and the two reactions at the bearing points were continuously measured with load cells. The deflection at the load points was measured with non-contact position sensors integrated into hydraulic jacks. Fig. 9 shows the transducers used to measure concrete displacements, deflections and inclinations to compare the measures with the previous tests performed in [41].

The strain gauges being placed at the steel reinforcement before casting were no more usable after the previous experimental campaign in [41]. Each strip was externally instrumented by a strain gauge at the middle beam cross-section height. To complete this instrumentation, digital image correlation (DIC) was used to obtain accurate measurements of the displacement field of specimens during all tests. More

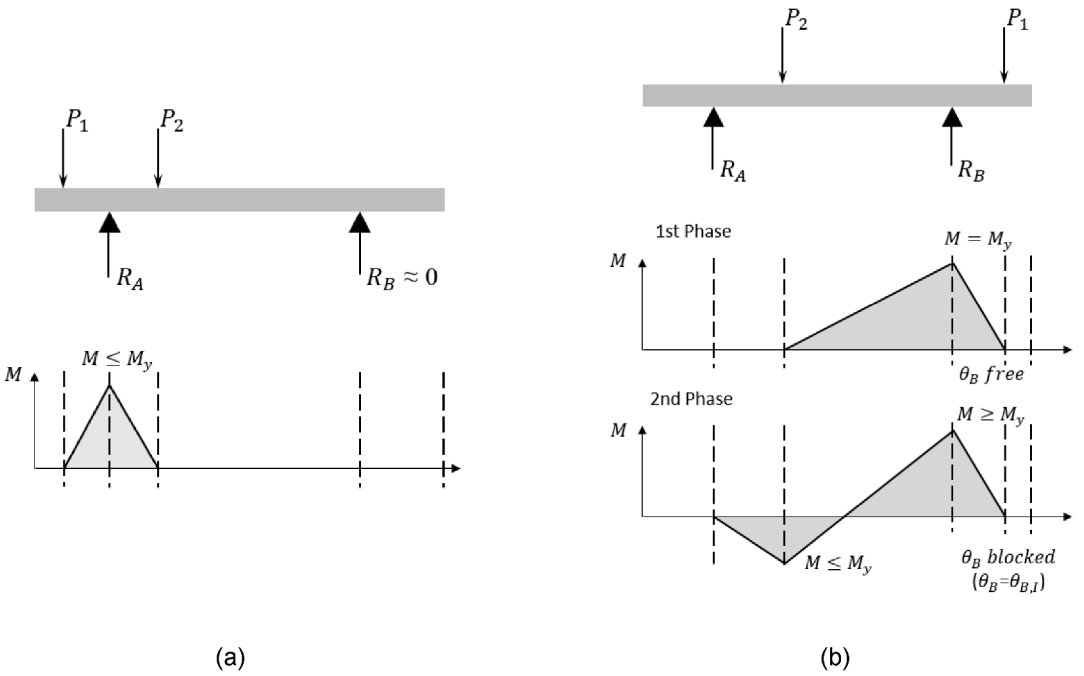

Fig. 8. Test procedure: (a) cantilever test, CE: (b) span test, SE. .
Adapted from [40]

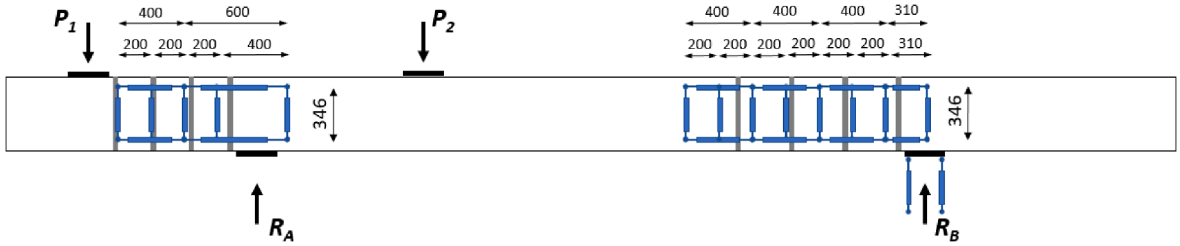

Fig. 9. Displacement transducers, adapted from [46] (dimensions in mm).

Table 3
Comparison of the main results at failure of the undamaged (previous experimental campaign) and *strengthened specimens.*

Spec.	Test	Failure mode	V_y(kN)	$P_{1,R}$(kN)	$P_{2,R}$(kN)	$M_{1,R}$(kNm)	$M_{2,R}$(kNm)	$V_{R,test}$(kN)	a(m)	a/d	$\psi_{b,R} - \psi_{b,f}$(mrad)	$w_{mean,R} - w_{mean,f}$(mm)
B12	B12C	V (B)	335.3	116.6		96.3		120.3	1	2.56	7.9	4.5
	R-B12C	V (B)*	338.0	243.8		196.3		247.4	1	2.56	9.8–12.6	9.1 – 14.5
B15	B15C	V (B)	334.3	276.8		225.4		280.5	1	2.57	11.0	ND
	R-B15C	V (A)**	336.7	354.1		284.1		357.7	1	2.57	31.4–54.5	1.4 – 3.1
B15	B15S	V (1 PH)	226.2	310.5	463.4	275.0	233.9	198.6	1.58	4.06	24.6	1.7
	R-B15S	M (2 PH)	226.9	373.3	620.2	327.1	325.1	253.5	1.49	3.82	57.1–62.9	1.9 – 2.1

Note: V (shear failure); M (bending failure); A (after yielding); B (before yielding); PH (plastic hinge); ND (data not available).
* Rupture of strip S3 in the anchoring zone (Fig. 7c).
** Rupture of strip S3 at the corner (Fig. 7d).

detailed information about photogrammetric measurements can be found in [40,46]. In addition, a high-speed camera was used to capture instantaneous beam failures.

4. Experimental results and discussion

This section presents the results obtained from the specimens tested during this experimental campaign and compares them to those obtained during the previous campaign on the same beams [41]. Table 3 includes the main results of the undamaged (previous experimental campaign) and strengthened tests (new experimental campaign), which are: the failure mode; the shear load corresponding to the full flexural strength (V_y); the loads applied at failure ($P_{1,R}$ and $P_{2,R}$); the bending moment at failure ($M_{1,R}$) at $d/2$ from the corresponding support (*A* for cantilever tests, Fig. 4a and Fig. 4b; *B* for the span test, Fig. 4c); the bending moment at failure ($M_{2,R}$) at $d/2$ from the section of load P_2 applied for the span test; the shear strength ($V_{R,test}$) provided by tests at failure at $d/2$ from the corresponding support (*A* for the cantilever tests and *B* for the span test). The control section, used to check shear, was located at $d/2$ from the applied load [47], and the bending moment and shear force included self-weight. The results were obtained at failure, which corresponded to the maximum load.

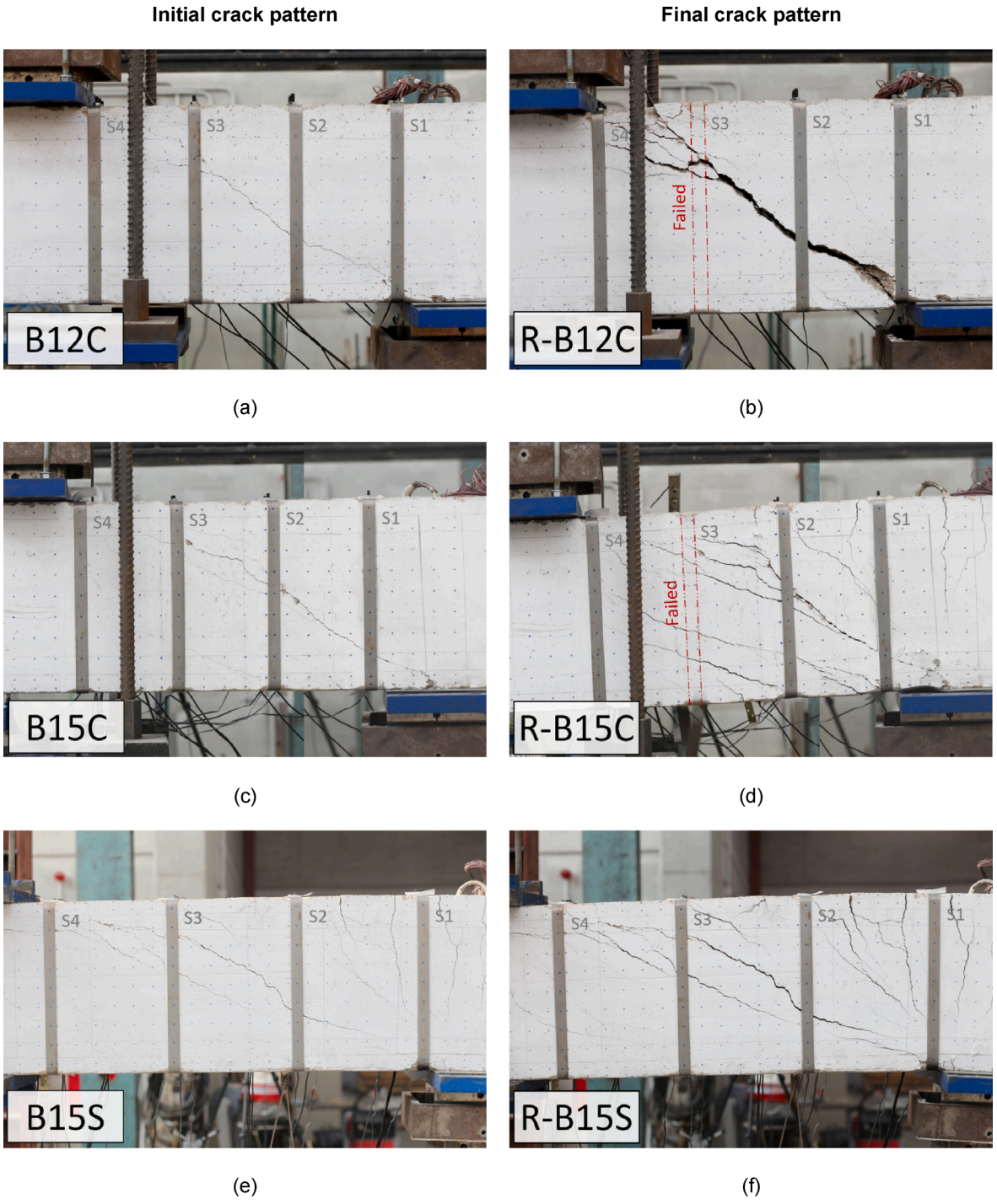

Fig. 10. Crack pattern on the strengthened beams. Before (left side) and after testing (right side): (a) B12C; (b) R-B12C; (c) B15C; (d) R-B15C; (e) B15S; (f) R-B15S.

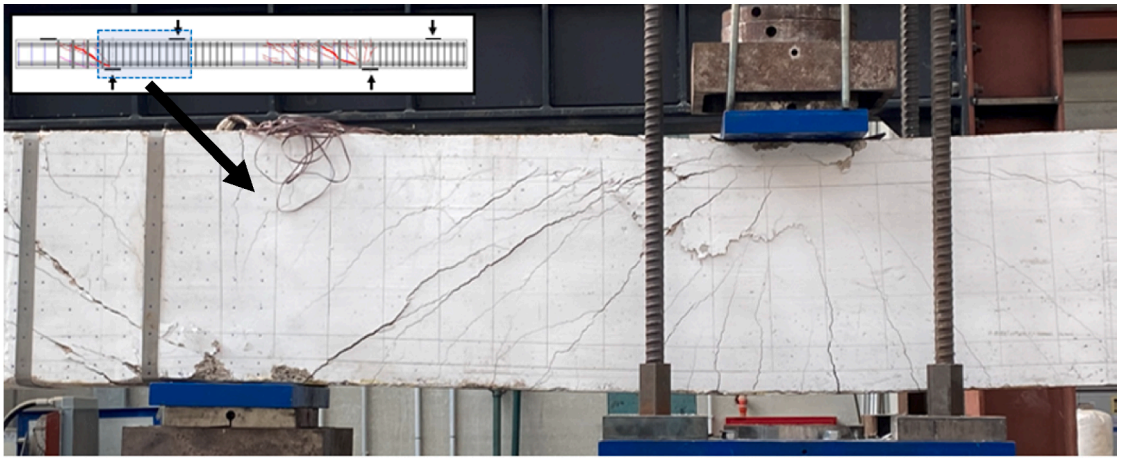

Fig. 11. Test R-B15S: Immediately before compression chord failure due to the increment in load P_2.

Table 3 also presents the equivalent shear span a ($a = M_{1,R}/V_{R,test} + d/2$), the shear span to the effective depth ratio a/d, the bending rotation values ψ_b and the mean of the CSC width w_{mean}. In the strengthened tests, the bending rotation and the mean of the CSC width corresponded to the increase in relation to the end of the initial tests. They are also displayed for two different test moments: at failure (maximum load) ($\psi_{b,R}$, $w_{mean,R}$) and at the end of the test ($\psi_{b,f}$, $w_{mean,f}$).

4.1. Crack pattern and failure modes

Fig. 10 shows the level of damage of the strengthened beams before and after testing. The damaged zones presented in the figure are those marked in Fig. 4. According to the analysis of the previously tested undamaged beams [41], cracking patterns at failure developed differently for the cantilever and continuous beam tests. In the cantilever tests of the undamaged beams (B12C and B15C), cracking started with vertical bending cracks near support A [41]. As the load increased, the CSC appeared directly as an inclined crack from the support point to the loading point, and its crack width increased until shear failure. The presence or absence of stirrups significantly influenced the cracking patterns. For the specimen with shear reinforcement (B15C test), cracks were more evenly distributed (Fig. 10c) than the specimen without stirrups (B12C test), for which strains were largely localised in a single critical shear crack (Fig. 10a). The average value of the different crack widths measured by DIC along the central branch of CSC at failure was 4.50 mm for the B12C test [48]. The data for the B15C test are not available (Table 3).

During the continuous undamaged beam test (B15S) [41], in the first loading phase, mainly bending cracks were observed. In the second test phase, the critical shear crack developed from a bending crack and progressed to shear failure (Fig. 10e). The average CSC width value at the first plastic hinge was 0.5 mm, and 1.7 mm at failure [48] (Table 3).

In the three tests performed with the strengthened beams, the width of the existing bending cracks of the damaged beams enlarged and new ones appeared with increased load. Relating to shear cracks, as specimen B12 did not contain internal shear reinforcement (stirrups), the vertical component of the CSC opening considerably increased to maximise the shear strength contribution of the external strips and the dowel effect of longitudinal reinforcement, which is feasible due to the high deformation capacity of Fe-SMA (Fig. 10b). That implied an increase in crack opening of 9.1 mm at maximum load and 14.5 mm at the end of the R-B12C test in relation to the initial crack opening present at the beginning of the test (approximately 0.75 mm).

However, in the other two tests (specimen with stirrups R-B15C and R-B15S), not only did the CSC width increase, but new shear cracks developed from the position of strips. In these cases, shear cracks were more distributed and the increase in CSC width was not as large as during test R-B12C. During test R-B15C (Fig. 10d), CSC width increased by 1.4 mm at failure and by 3.1 at the end of the test compared to the crack opening at the beginning of the test (approximately 1 mm). During the continuous beam test (R-B15S), the increment in CSC width was 1.89 mm at failure and 2.1 at the end of the test during the initial remaining crack opening of approximately 1.40 mm (Fig. 10f).

The failure mode and shear load corresponding to the full flexural strength (V_y) of the undamaged (previous experimental campaign) and strengthened specimens are presented in Table 3. Full flexural strength included the beam's self-weight. This shear force V_y represents the theoretical value at which longitudinal reinforcement was the yielded during the CE tests and the second plastic hinge development upon load P_2 during the SE tests. In the strengthened beams, this reference value (V_y) was used to determine if failure was achieved before (B) or after (A) yielding longitudinal reinforcement for the CE test, or after the second plastic hinge developed (2 PH) for the SE test. In the tests done with the undamaged beams [41], the strain gauges placed on longitudinal tensile reinforcement were used to determine these failure modes. However, these strain gauges did not work in the tests done with the strengthened beams.

During the CE tests of the undamaged beams (B12C and B15C), shear failure developed before longitudinal reinforcement yielded ($V_{R,test} < V_y$, see Table 3) [41]. However during the SE test of the undamaged beams (B15S), shear failure developed after yielding of the top longitudinal reinforcement in tension and with increasing shear force, along with the development of plastic hinge rotations [41]. No second plastic hinge developed during test B15S ($V_{R,test} < V_y$, see Table 3).

Yet after strengthening, shear failure in the R-B12C test was produced after strip S3 broke off in the anchoring zone (Fig. 7c and Fig. 10b). This failure was achieved before longitudinal reinforcement yielded, which was also the case during the original test (B12C) ($V_{R,test} < V_y$, Table 3). Test R-B15C failed directly due to the rupture of strip S3 at the corner (Fig. 10d and Fig. 7d). However in this case, shear failure occurred after yielding of the longitudinal reinforcement ($V_{R,test} > V_y$, Table 3).

During the SE test, a plastic hinge on support B was generated by applying load P_1 in both cases; the original and strengthened tests. For the original SE test (B15S), shear failure occurred before the development of the second hinge. However, when external Fe-SMA strips were

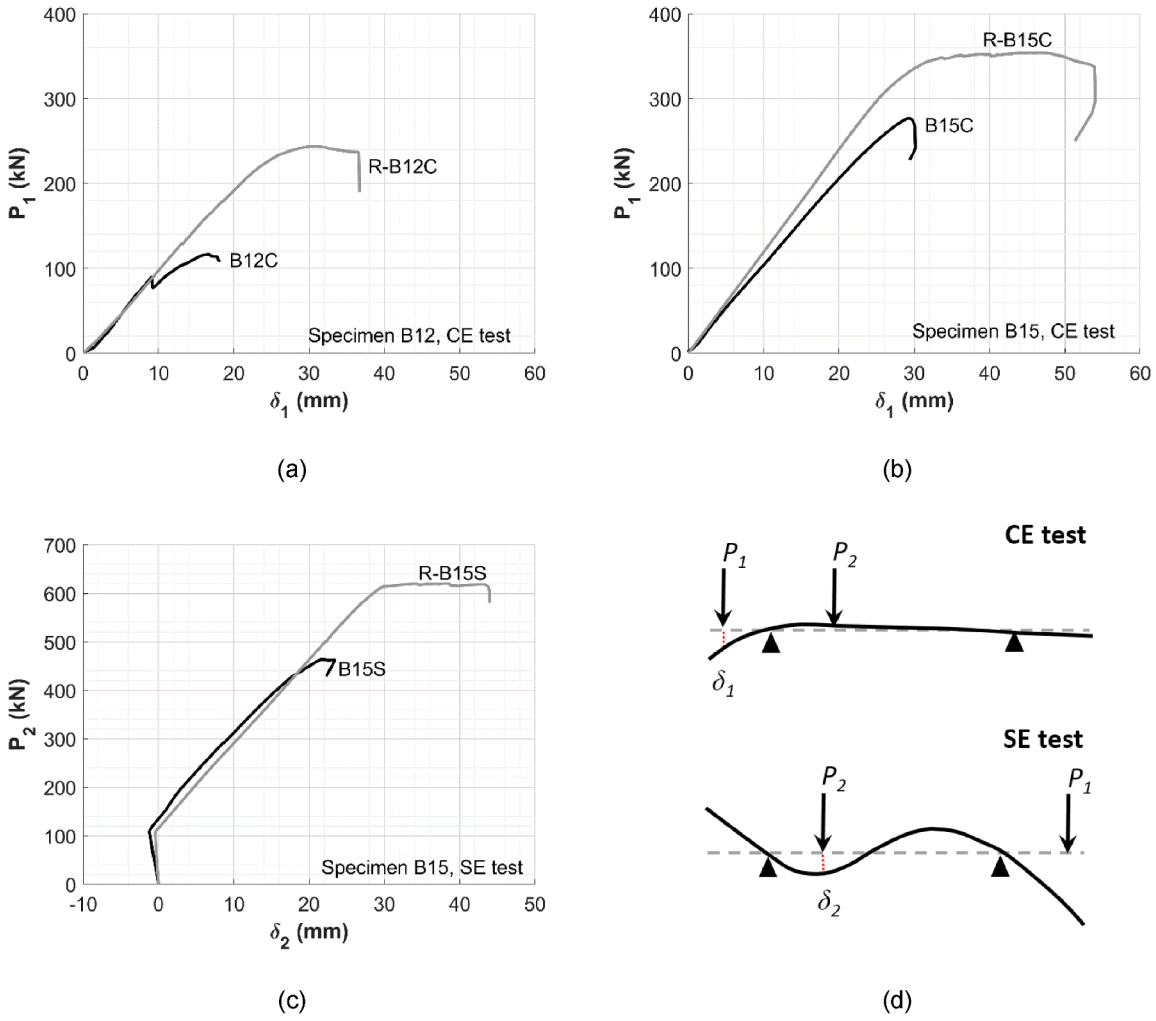

Fig. 12. Comparison of the load–deflection curves between the tested undamaged and strengthened beams: (a) CE tests on specimen B12; (b) CE tests on specimen B15; (c) SE tests on specimen B15; (d) loading-displacements scheme for both test configurations.

employed, the beam was able to develop the second hinge during test R-B15S by load P_2, and the shear force on the beam increased on both supports A and B in the second phase ($V_{R,test} > V_y$, Table 3). Finally, the beam collapsed due to the failure of the compression chord on the non-strengthened span (Fig. 11).

4.2. Load-deflection behaviour

Fig. 12 shows the general behaviour of all tests when referring to shear strength, initial stiffness and post-peak behaviour. The vertical axes represent the load measured by the load cell and the horizontal axes correspond to the vertical displacement of the corresponding actuator, with load P_1 and displacement δ_1 for the cantilever test (CE), load P_2 and δ_2 for the span test (SE) (Fig. 12d).

In the three tests, the load–deflection curves of the initial beams exhibit brittle shear failure with a sharp drop in load after reaching the maximum load. However, the use of Fe-SMA strips not only enhances the shear strength of the beams but also improves their ductility. The beams' initial shear strength is restored and overcome in all three tests.

In the CE tests, the P- δ curves show one branch in the previous tests with the undamaged beams. These curves reflect the linear increase in P_1 and the large cantilever deflection until shear failure with no yielding of the top tensile reinforcement [41]. However, after strengthening of these beams and retesting, shear failure occurs on a second branch. Specimen B12 reaches load $P_1 = 116.6$ kN during the initial test (B12C), and 243.8 kN after being strengthened and retested (R-B12C). A 109% increase is achieved (more than double the shear strength capacity). With specimen B12, the shear failure mode is achieved before yielding of the longitudinal reinforcement for both tests with the undamaged (B12C) and the strengthened beam (R-B12C). Specimen B15 reaches load $P_1 = 276.8$ kN during the initial test (B15C), and 354.1 kN after having been strengthened and retested (R-B15C). A 28% increase is accomplished. However in this case, after beam strengthening, shear failure occurs on a second branch after the yielding of tensile reinforcement.

For the SE test, the P- δ curve shows two branches for the previous test with the undamaged beam. The first branch corresponds to the first test phase. In this phase, the branch has a negative slope and the increase in δ_2 is negative because the load applied in this phase is P_1. In the second phase, the second branch of the curve reflects the increase in P_2 and marks beam deflection; that is, after the first plastic hinge develops on support B and before yielding of the bottom longitudinal (tensile) reinforcement under the section where P_2 load is applied. On this ascending branch, the beam fails in shear during the previous test.

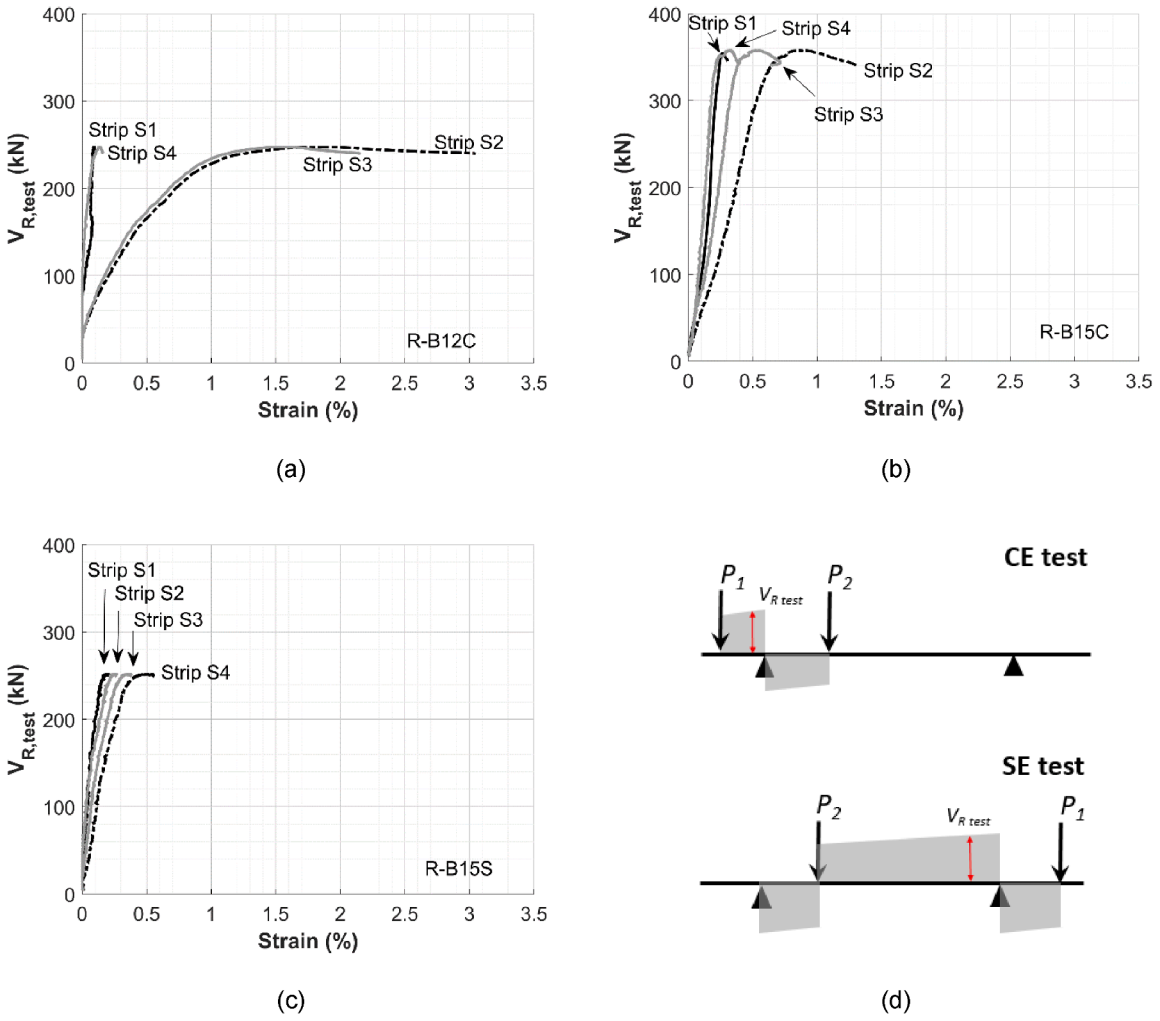

Fig. 13. Strains measured on external Fe-SMA strips: (a) CE tests on specimen B12; (b) CE tests on specimen B15; (c) SE tests on specimen B15; (d) shear diagram for both test configurations.

However, after strengthening the beam and retesting, compression chord failure occurs on a third-shaped branch after the second plastic hinge has developed. Specimen B15 reaches load $P_2 = 463.4$ kN during the previous test (B15S), and 620.2 kN after being strengthened and retested (R-B15S). A 34% increase is achieved.

The strengthening system using Fe-SMA strips applied to the damaged RC beams allows their initial strength to increase and confers them ductility, even when changing the failure mode.

4.3. Strain in external strips

As strips were not bonded with concrete, the strains measured by strain gauges had to remain constant through the vertical segments. Fig. 13 shows the curves that related the strain measured on strips by the attached strain-gauges and the shear force at the beam in the study area. The control section to check shear was located at $d/2$ from the applied load, which included self-weight as shown in Fig. 13d.

In all the specimens, the strain gauges measures on the central strips S2 and S3 were higher than onf the extreme strips S1 and S4 (see the position of strips in Fig. 4). This confirms that central strips contribute more to shear strength, despite extreme strips also enhance load transmission. The higher strain of these strips occurred in specimen B12 because the cantilever of this beam had no transversal reinforcement. In the other CE test, specimen B15 and strips S2 and S3 also reached significant strains. Nevertheless, the lower strains on strips occurred during the SE test, where no strip failed.

Previous studies by the authors [34,36] detected that those strips started to work when shear cracks appeared on beams. In those studies, when strips were activated, initial tensile stress was introduced into beams before the test started. This stress remained constant until small shear cracks started appearing. The generated confinement delayed the first shear crack from appearing. However, as the tested beams were already considerably cracked during the present experimental campaign, work with strips started for low load levels.

4.4. Bending rotations

Table 3 shows the bending rotation values (ψ_b) at failure for the undamaged specimens [41], and also at failure and at the end of tests for the strengthened specimens. Bending rotation was obtained by calculating the bending curvatures in different sections by integrating along the beam length where the critical shear crack (CSC) developed, approximately to $2d$ from the support section (support A for the CE tests and B for the SE test, Fig. 4). Bending curvatures were calculated by digital image correlation (DIC) from the longitudinal strains of the top and bottom beam fibres [41]. Therefore, this rotation corresponded to

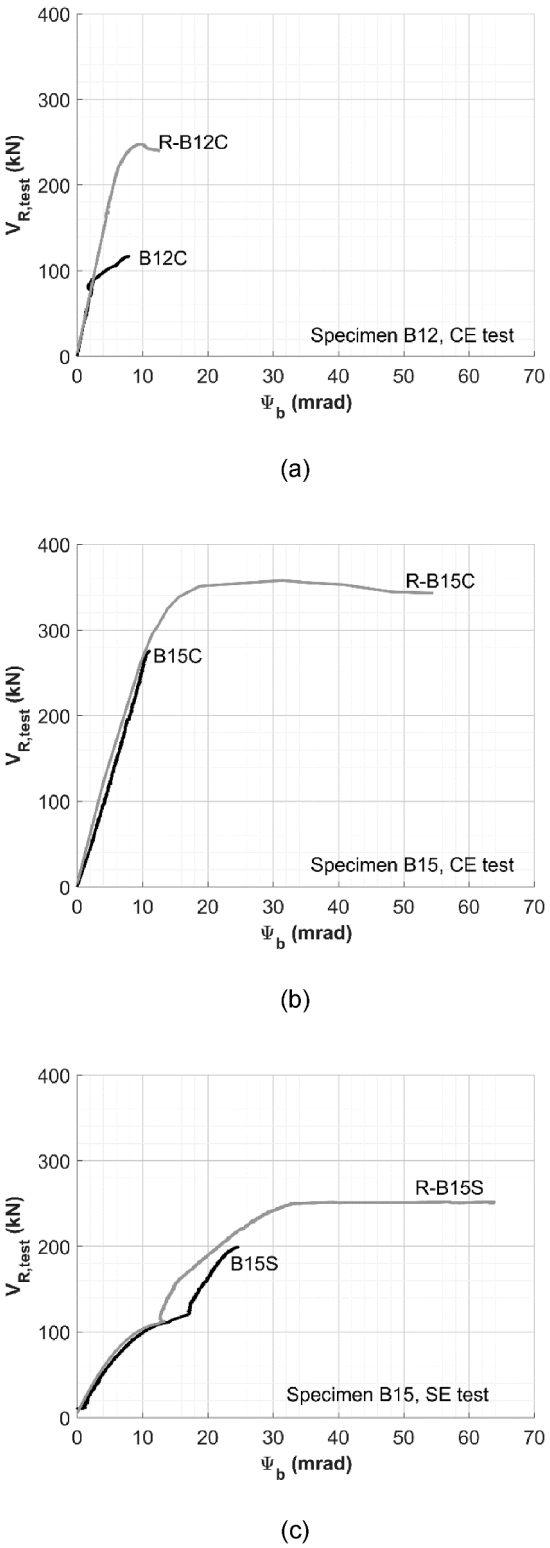

Fig. 14. Bending rotation evolution versus shear force: (a), (b), (c) bending rotation evolution versus shear force for each specimen during the undamaged and strengthened tests.

bending deformation independently of shear crack evolution. The shear represented in Fig. 14 is located at $d/2$ from the applied load and includes self-weight.

It is important to highlight that, due to the previous damage to specimens, the rotation values of the strengthened specimens corresponded to the increase in the remnant deformations after the unloading during previous tests. The incremented bending rotation achieved at the end of tests by the strengthened specimens was 1.59-, 4.95- and 2.56-fold in relation to the bending rotation obtained in the original tests for tests R-B12C, R-B15C and R-B15S, respectively.

Fig. 14 shows the rotation development for each test versus the shear force supported by beams. As we can see, strengthening did not change beams' stiffness in relation to bending rotations, and the undamaged and strengthened tests present similar slopes of curves. Test R-B12C presents a lesser increase in bending rotation because failure occurred longitudinal reinforcement was yielded ($V_{R,test} < V_y$, Table 3). The significant displacement at load P_1 seen in Fig. 10a for this test was primarily due to the vertical separation displacement between the two parts of the crack (Fig. 10a and Fig. 10b) and not to a bending rotation of the specimen in Fig. 14a. However, specimen R-B15 showed a significant increase in bending rotation capacity during both tests (cantilever and span test) after being strengthened with external Fe-SMA strips (Fig. 14b and Fig. 14c).

During test R-B15C, this increase was due to the yielding of longitudinal reinforcement ($V_{R,test} > V_y$, Table 3), while during test R-B15S test, the development of the second plastic hinge ($V_{R,test} > V_y$, Table 3) allowed bending rotation to increase with constant shear strength. It must be pointed out that the slope of the support section in the second phase of test R-B15S remained constant due to the block of the support. During both R-B15C and R-B15S, ductile behaviour was observed, but not during the undamaged tests (B15C and B15S) as a consequence of either the yielding of longitudinal reinforcement (R-B15C) or the development of the second plastic hinge (R-B15S), along with improved shear strength due to the external Fe-SMA strips.

4.5. Shear strength components

This section presents an estimation of the contribution of different shear strength components to the tested strengthened beams and a comparison to the initial tests. There were three components: 1) the shear strength provided by concrete (V_c); 2) the shear strength provided by shear reinforcement (V_s); 3) the shear strength provided by the external Fe-SMA strips (V_{SMA}). The component provided by concrete included the contribution of the compression chord, aggregate interlock, residual tensile strength and the dowel effect of longitudinal reinforcement. The shear strength for each component obtained during tests is presented in Table 4.

The shear strength provided by shear reinforcement (V_s) and the external strips (V_{SMA}) was calculated as the sum of the tensile forces of all the stirrups and external strips crossed by the CSC, according to the equations below:

$$V_s = \sum \sigma_{sw} \hat{A} \cdot \frac{\emptyset^2 \hat{A} \cdot \pi}{4} \quad (1)$$

$$V_{SMA} = \sum \sigma_{SMA} \hat{A} \cdot A_{strip} \quad (2)$$

Table 4
Shear strength components of the undamaged (previous experimental campaign) and strengthened specimens.

Spec.	Test	$V_{R,test}$(kN)	$V_{s,test}$(kN)	$V^{inf}_{SMA,test} - V^{sup}_{SMA,test}$ (kN)	$V^{inf}_{c,test} - V^{sup}_{c,test}$(kN)
B12	B12C	120.3	–	–	120.3
	R-B12C	247.4	–	116.8 – 120.4	127.0 – 130.6
B15	B15C	280.5	174.0	–	106.5
	R-B15C	357.7	177.8	84.4 – 109.2	70.7 – 95.5
B15	B15S	198.6	174.5	–	24.1
	R-B15S	253.5	174.5	66.6 – 79.0*	0 – 12.5

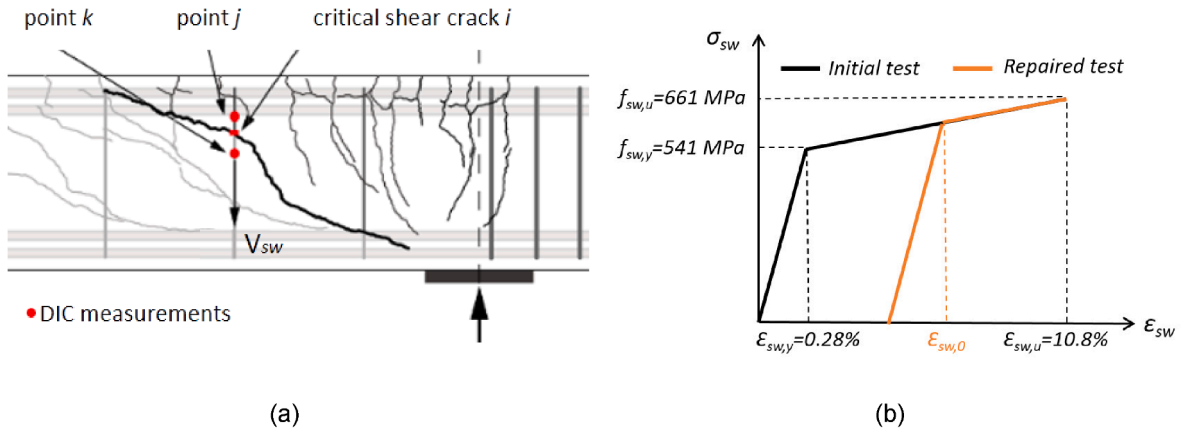

Fig. 15. (a) Vertical crack opening of the critical shear crack by DIC [40]; (b) adapted stress–strain relation of stirrups' steel according to the strain in the initial test.

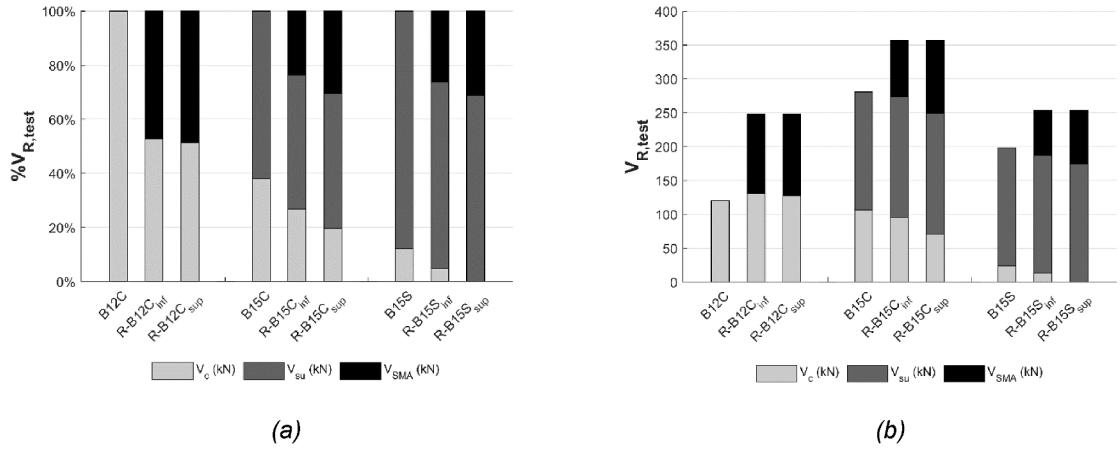

Fig. 16. Contribution of the different shear strength components in the undamaged and strengthened tests. (a) contribution of each component as a %; (b) absolute value of each component.

where Ø is the diameter of the transversal bar, σ_{sw} is the normal stress for a single stirrup (two branches per stirrup), A_{strip} is the area of strips (two branches per strip) and σ_{SMA} is the tensile stress for the activated strips with constrained recovery strain (two branches per strip).

Normal stress at stirrups has been calculated by following the procedure proposed by Campana et al.[49]. For this, the vertical crack opening at the location where the crack intercepted a stirrup is obtained by means of the DIC displacement measurements from two points vertically aligned with the stirrup (one on each side of the crack) (Fig. 15a). More details of the calculation can be found in [40,46]. A bilinear hardening stress–strain relationship of steel (Fig. 15b) has been adapted to estimate the remaining strains of the stirrups after the unloading process of the initial tests, as the stirrups yielded before failure [41]. The number of stirrups accounted for calculating the shear strength component depends on the crack shape. Three stirrups where considered for the specimen B15. Additional stirrups are intercepted by the propagation of the horizontal branch at the location of the longitudinal tensile reinforcement. Nevertheless, those transversal elements are not considered in the contribution of the shear reinforcement, their eventual contribution comes from dowelling forces [3,40,49].

Estimates of the stress reached by each strip were done based on the strain measurements taken by the strain gauges placed on strips (Fig. 13) and the strain–stress curve of the strengthening material (Fig. 3). However, given the challenge of determining the recovery constraint strain in the external Fe-SMA strips, the stress in each strip was calculated after taking into account two extreme hypotheses: perfect contact between strips, concrete, and anchorage, to allow the generation of recovery stresses up to 350 N/mm^2 to be generated, and free recovery strain with no recovery stresses (Fig. 3a).

Consequently, the contributions by the external Fe-SMA strips ($V^{inf}_{SMA,test} - V^{sup}_{SMA,test}$) were calculated as a range of values after taking into account both the free recovery strain or constraint recovery strain hypotheses. The number of external strips was used for calculating the shear strength components, which depend on crack shape, and follow the same criterion as stirrups, as described above. Two external Fe-SMA strips were intercepted by the diagonal part of the critical shear cracks in all cases.

Finally, the concrete contribution range ($V^{inf}_{c,test} - V^{sup}_{c,test}$), as regards the two extreme situations of the component provided by the external Fe-SMA strips ($V^{inf}_{SMA,test} - V^{sup}_{SMA,test}$), was calculated as the difference between the total shear strength and the sum of the other components when considering the constraint recovery strain in the Fe-SMA strips ($V^{inf}_{c,test} = V_{R,test} - V_{s,test} - V^{sup}_{SMA,test}$) and the free recovery strain in the Fe-SMA strips ($V^{sup}_{c,test} = V_{R,test} - V_{s,test} - V^{inf}_{SMA,test}$). Fig. 16 shows the shear force provided by the different components during all the tests.

It is noteworthy that the estimated inferior shear strength value of

concrete for test R-B15S was negative when accounting for the maximum contribution of SMA strips (marked in Table 4 by an asterisk). This result is makes physically no sense, and necessitates the imposition of an upper limit to the actual shear contribution of SMA strips to preclude any negative values of the concrete shear strength in this scenario. This signifies that the actual shear contribution of strips cannot reach the upper limit of the previously considered range.

The results show that the contribution of concrete decreased from the previous tests to the strengthened tests, and even disappeared for the SE test when $V_{SMA,test}^{sup}$ was considered. Similar behaviour was seen during a previous experimental campaign on RC beams with superelastic (Ni-Ti) internal shear reinforcement [50], in which the very high damage level in concrete nullified its contribution, but shear reinforcement was able to keep the two concrete blocks separated by the CSC. In the present tests, the huge CSC opening hindered shear transfer by aggregate interlock. Therefore, the shear strength provided by concrete was due mainly to the dowel effect of longitudinal reinforcement and/or the shear transferred through the compression zone thanks to the vertical confinement stresses created by the external strips. For the shear strength provided by stirrups, the shear load transference crossed by a CSC in both tests was estimated (before and after applying strengthening). A clear increase in shear strength occurred on account of the external Fe-SMA strips.

During test R-B12C, a cantilever test without stirrups, the shear strength provided by the external Fe-SMA strips increased the shear strength versus the initial test to a double load. The contribution of the external Fe-SMA strips during this test represented approximately 50%, and the other 50% provided by other mechanisms, mainly the dowel effect of longitudinal reinforcement, were both upper and lower. During cantilever test R-B15C with transversal reinforcement, the shear strength provided by stirrups represented about 49.7% of shear strength, and between 23.6% and 30.5% was provided by the external Fe-SMA strips. Therefore, concrete contributed only between 19.8% and 26.7%. With test R-B15S, shear strength was almost completely provided by stirrups and the external Fe-SMA strips because the concrete's contribution was negligible. The shear strength provided by stirrups and strips was about 68.9% and between 26.3% and 31.1%, respectively.

5. Comparing the test results to existing code provisions

A comparison between the different shear procedures was made to estimate the shear strength of the tested beams. The considered procedures were the compression chord capacity model (CCCM) [1], Model Code 2010 [9] (Level III Approximation for specimens with transverse reinforcement and Level II Approximation for the specimen without transverse reinforcement), ACI CODE-318–19 [8] and Eurocode 2 [11].

The CCCM is a simplified model for the shear strength prediction of reinforced and prestressed concrete members, both with and without transverse reinforcement in different cross-sections. It derives as a simplification of the multi-action shear model (MASM) [4]. Both models are based on classic mechanics, but the MASM proposes explicit equations for different shear transfer actions. The CCCM considers that the main resisting action in the considered failure state is the shear transferred by the compression chord. It also includes an independent equation to consider the increment in shear resisted by concrete, caused by strip confinement on the compression chord, termed Δv_{cu} (see [34,39,44,51]). This term can be considered because the external strips fully wrapped the beam. However, it should be interpreted carefully according to the initial damage of the strengthened specimens. MC2010 Level III was used in the initial experimental programme and provided the least scattered results in the different procedures [41]. For the MC2010, ACI CODE-318–19 [8] and Eurocode 2 [11] calculations, the shear strength provided by the external strips was taken as additional transversal reinforcement.

The main results of that comparison are summarised from Table 5 to

Table 5
Predictions by the CCCM [1].

Spec.	Test	$V_{R.test}$(kN)	V_y(kN)	V_c(kN)	V_c^{conf}(kN)	V_s(kN)	V_{SMA}(kN)	V_{CCCM}(kN)	V_R(kN)	$\frac{V_{R.test}}{V_R}$
B12	B12C	119.4	334.4	105.2	–	–	–	105.2	105.1	1.14
	R-B12C	246.5	337.1	119.2	30.3	–	80.9	230.4	230.4	1.07
B15	B15C	279.6	333.4	99.6	–	125.8	–	225.4	225.4	1.24
	R-B15C	356.8	335.8	110.5	30.8	124.1	80.9	342.7	335.8	1.06
B15	B15S	197.7	225.3	90.6	–	125.8	–	216.4	216.4	0.91
	R-B15S	252.6	226.0	106.8	21.4	125.8	58.2	312.1	226.0	1.12
	Undamaged tests									
Average										1.10
Coefficient of Variation (%)										15.23
	Strengthened tests									
Average										1.08
Coefficient of Variation (%)										2.76

Table 6
Predictions by Model Code 2010 [9].

Spec.	Test	$V_{R.test}$(kN)	V_y(kN)	V_c(kN)	V_s(kN)	V_{SMA}(kN)	$V_{MC-2010}$(kN)	V_R(kN)	$\frac{V_{R.test}}{V_R}$
B12	B12C	119.4	334.4	106.2	–	–	106.2	106.2	1.12
	R-B12C	246.5	337.1	65.8	–	156.3	222.1	222.1	1.11
B15	B15C	279.6	333.4	45.5	174.3	–	219.8	219.8	1.27
	R-B15C	356.8	335.8	40.0	145.8	131.2	317.0	317.0	1.13
B15	B15S	197.7	225.3	41.2	144.4	–	185.6	185.6	1.06
	R-B15S	252.6	226.0	42.3	145.8	94.3	282.4	226.0	1.12
	Undamaged tests								
Average									1.15
Coefficient of Variation (%)									9.24
	Strengthened tests								
Average									1.12
Coefficient of Variation (%)									0.70

Table 7
Predictions by ACI CODE-318-19 [8].

Spec.	Test	$V_{R,test}$(kN)	V_y(kN)	V_c(kN)	V_s(kN)	V_{SMA}(kN)	V_{ACI}(kN)	V_R(kN)	$\frac{V_{R,test}}{V_R}$
B12	B12C	119.4	334.4	92.9	–	–	92.9	92.9	1.28
	R-B12C	246.5	337.1	104.1	–	95.2	199.3	199.3	1.24
B15	B15C	279.6	333.4	88.5	105.8	–	194.3	194.3	1.44
	R-B15C	356.8	335.8	97.2	105.8	95.2	298.1	298.1	1.20
B15	B15S	197.7	225.3	88.5	105.8	–	194.3	194.3	1.02
	R-B15S	252.6	226.0	97.2	105.8	68.4	271.4	226.0	1.12
	Undamaged tests								
Average									1.25
Coefficient of Variation (%)									17.10
	Strengthened tests								
Average									1.18
Coefficient of Variation (%)									5.14

Table 8
Predictions by Eurocode 2 [11].

Spec.	Test	$V_{R,test}$(kN)	V_y(kN)	V_c(kN)	V_s(kN)	V_{SMA}(kN)	V_{EC2}(kN)	V_R(kN)	$\frac{V_{R,test}}{V_R}$
B12	B12C	119.4	334.4	114.7	–	–	114.7	114.7	1.04
	R-B12C	246.5	337.1	–	–	214.1	214.1	214.1	1.15
B15	B15C	279.6	333.4	–	233.8	–	233.8	233.8	1.20
	R-B15C	356.8	335.8	–	236.0	212.5	448.5	335.8	1.06
B15	B15S	197.7	225.3	–	233.8	–	233.8	225.3	0.88
	R-B15S	252.6	226.0	–	236.0	152.7	388.7	226.0	1.12
	Undamaged tests								
Average									1.04
Coefficient of Variation (%)									15.34
	Strengthened tests								
Average									1.11
Coefficient of Variation (%)									4.04

Table 8 for the predictions by the CCCM, MC2010, ACI CODE-318–19 [8] and Eurocode 2 [11]. Column $V_{R,test}$ shows the shear strength in the control section. The control section was placed at a distance d from the edge of the supports for all the considered methods. Note that the $V_{R,test}$ values presented herein are slightly lower than those in Table 4, where values are taken at the support axis. Column V_y presents the predicted shear force at bending failure. This value is considered a limit when the shear strength predicted by any model (V_{CCCM}, V_{MC}, V_{ACI}, V_{EC2}) is higher than V_y, as was the case, for example, for the strengthened B15 specimen (R-B15S) for all the considered shear procedures. Note that column V_R present the minimum value between that of the shear prediction and V_y. Average laboratory values were considered according to the compressive strength at the time of the previous experimental programme, rather than design values, for the material strength parameters. Shear strength predictions were also calculated (for the strengthened specimens) for the compressive strength values at the time of the strengthened beam tests so that these values would allow us to obtain fewer conservative predictions. With the external Fe-SMA strips, the material's yielding strength was substituted by the measured 0.20% proof stress, 626.2 N/mm^2 (Fig. 3a). This value is slightly 4.7% higher than the design value recommended by the Fe-SMA manufacturer, which approximately equals 598 N/mm^2 (460 N/mm^2 including a safety factor of 1.3 [52]).

The predictions by all the shear procedures gave satisfactory results, which should be considered with caution because more tests are needed to improve their statistical significance. Moreover, the behaviour of two retrofitted beams (R-B15C and R-B15S) could have been influenced by the yielding of longitudinal reinforcement because for these two tests: $V_{R,test} > V_y$.

6. Conclusions

The feasibility of strengthening shear-damaged reinforced concrete beams by using external iron-based shape memory alloys strips is experimentally proven in this paper. An experimental campaign of three tests performed over two real-scale beams with a substantial level of damage is analysed and compared to the rest of those beams developed in a previous study before being strengthened.

During previous tests, load–deflection curves exhibited brittle shear failure with a sharp drop in load after reaching the maximum load. However, the strengthening system allowed their initial strength to increase, which conferred them ductility, and even changed the failure mode. It is important to highlight that, thanks to concrete's active confinement caused by the shape memory effect of strips, the strengthening strips started to work immediately after they were applied. It is also noteworthy that the cracks produced during the previous experimental campaign were not really repaired (no crack injections or use of repairing mortars). When comparing the experimental results of the strengthened beams to that of the original undamaged beams, shear strength increased by between 28% and 34% for the specimens with the internal stirrups and by 109% for the specimen without the internal stirrups. The increment in the bending rotation at the end of the test achieved by the strengthened specimens was also noteworthy, which was between 1.59- and 4.95-fold that of the undamaged ones. During both the strengthened tests carried out on specimen B15 (with shear reinforcement), shear failure occurred after the yielding of longitudinal reinforcement.

The analysis of the results showed that concrete contribution to shear strength reduced from the previous tests to the strengthened tests. The huge critical shear crack opening hindered the shear transfer by aggregate interlock. With the cantilever test without stirrups, the contribution of the external Fe-SMA strips represented approximately 50% of shear strength. For the cantilever test with transversal reinforcement, the

shear strength provided by stirrups represented about 49.7% of shear strength and between 23.6% and 30.5% was provided by the external Fe-SMA strips. Therefore, according to the followed methodology, only between 19.8% and 26.7% was contributed by concrete and other mechanisms. With the continuous beam, concrete contribution was negligible, and shear strength was completely contributed by stirrups (68.3%) and the external Fe-SMA strips (26.3–39.7%).

The shear strength of the undamaged and strengthened specimens was compared to the predictions by the Compression Chord Capacity Model (CCCM) and the shear procedures included in Model Code 2010, ACI318-19 and Eurocode 2. As tests were few, the results of these comparisons should be cautiously considered. All the procedures led to general conservative and satisfactory results.

This research work concludes that the strengthening technique done with Fe-SMA strips to wrap beams and to anchor themselves using screws and nuts can be successfully applied to strengthen reinforced concrete beams damaged upon shear by increasing the ductility of the shear failures caused after the yielding of longitudinal reinforcement. Despite the positive results, this research was conducted as a proof test. Therefore, further research by varying different parameters should be carried out to study their influence on both shear strength and rotation capacity, and to prevent premature strip failure.

In the context of practical applications, this study underscores the necessity for further adaptations of the proposed shear-strengthening technique. Particularly in already-constructed structures, where access to the top side of beams might be limited, alternative anchoring methods that maintain the demonstrated effectiveness of Fe-SMA strips might need to be developed. Future research should focus on these adaptations, aiming to translate the promising results from this proof-of-concept study into more practical applications. Therefore, while this research provides a pivotal step in the process of developing and refining a new method of shear strengthening, it also highlights the importance of continuous innovation and development in the field to overcome real-world constraints.

CRediT authorship contribution statement

Celia Traver: Writing – review & editing, Writing – original draft, Visualization, Validation, Resources, Investigation, Formal analysis. **Joaquín G. Ruiz-Pinilla:** Writing – review & editing, Writing – original draft, Visualization, Validation, Supervision, Resources, Methodology, Investigation, Formal analysis. **Andrea Monserrrat:** Writing – review & editing, Validation, Resources, Methodology, Investigation, Formal analysis. **Luis A. Montoya-Coronado:** Writing – review & editing, Writing – original draft, Visualization, Validation, Resources, Methodology, Investigation, Formal analysis. **Pedro F. Miguel:** Writing – review & editing, Supervision, Project administration, Methodology, Funding acquisition. **Carlos Ribas:** Writing – review & editing, Project administration, Methodology, Funding acquisition. **Antoni Cladera:** Writing – review & editing, Writing – original draft, Supervision, Project administration, Methodology, Funding acquisition, Formal analysis, Conceptualization. **José L. Bonet:** Writing – review & editing, Writing – original draft, Supervision, Project administration, Methodology, Funding acquisition, Conceptualization.

Declaration of Competing Interest

The authors declare that they have no known competing financial interests or personal relationships that could have appeared to influence the work reported in this paper.

Data availability

Data will be made available on request.

Acknowledgements

The authors would like to thank the financial support provided by Grants: PID2021-126397OB-I00, PID2021-123701OB-C22, BIA2015-64672-C4-4-R and BIA2015-3 64672-C4-3-R by MCIN/AEI/10.13039/501100011033 and by “ERDF A way of making Europe.”; RTI2018-099091-B-C21-AR and RTI2018-099091-B-C22 by MCIN/AEI/10.13039/501100011033 and by “ERDF A way of making Europe” and BIA2015-64672-C4-4-R and BIA2015-64672-C4-3-R (AEI / FEDER, UE); and TED2021-129358B-I00 and TED2021-130272B-C22 funded by MCIN/AEI/ 10.13039/501100011033 and by the European Union NextGeneration EU/PRTR”. The Regional Valencian Government also supported this research with Project AICO/2020/295. Andrea Monserrat is supported by the Ministry of Universities (Spain) with the Recovery, Transformation and Resilience Plan (RD 289/2021 and order UNI/551/2021) funded by NextGenerationEU. The authors thank the Spanish Ministry of Science and Innovation for Grant FPU18/03310 that supported Celia Traver Abella. This research work was undertaken at the Concrete Science and Technology University Institute (ICITECH) of the Universitat Politècnica de València (UPV; Spain), with concrete supplied by Caplansa. They also appreciate the contribution of the re-fer AG Strengthening Solution Company, which provided the memory steel (Fe-SMA strips).

References

[1] A. Cladera, A. Marí, J.M. Bairán, C. Ribas, E. Oller, N. Duarte, The compression chord capacity model for the shear design and assessment of reinforced and prestressed concrete beams, Struct. Concr. 17 (2016) 1017–1032, https://doi.org/10.1002/suco.201500214.
[2] T. Zhang, P. Visintin, D.J. Oehlers, Shear strength of RC beams without web reinforcement, Aust. J. Struct. Eng. 17 (2016) 87–96, https://doi.org/10.1080/13287982.2015.1122502.
[3] P. Huber, T. Huber, J. Kollegger, Investigation of the shear behavior of RC beams on the basis of measured crack kinematics, Eng. Struct. 113 (2016) 41–58, https://doi.org/10.1016/j.engstruct.2016.01.025.
[4] A. Marí, J. Bairán, A. Cladera, E. Oller, C. Ribas, Shear-flexural strength mechanical model for the design and assessment of reinforced concrete beams, Struct. Infrastruct. Eng. 11 (2015) 1399–1419, https://doi.org/10.1080/15732479.2014.964735.
[5] F. Cavagnis, M. Fernández Ruiz, A. Muttoni, A mechanical model for failures in shear of members without transverse reinforcement based on development of a critical shear crack, Eng. Struct. 157 (2018) 300–315, https://doi.org/10.1016/j.engstruct.2017.12.004.
[6] P.M. Calvi, E.C. Bentz, M.P. Collins, Pure mechanics crack model for shear stress transfer in cracked reinforced concrete, ACI Struct. J. 114 (2017) 545–554, https://doi.org/10.14359/51689460.
[7] L.A. Montoya-Coronado, C. Ribas, J.G. Ruiz-Pinilla, A. Cladera, Time-history analysis of aggregate interlock in reinforced concrete beams without stirrups, Eng. Struct. 283 (2023) 115912.
[8] ACI Committee, 318-19 Building Code Requirements for Structural Concrete and Commentary, 318-19 Building Code Requirements for Structural Concrete and Commentary. (2019). https://doi.org/10.14359/51716937.
[9] M. Code, Model code 2010: final draft, 2010.
[10] CSA Committee A23.3, Design of concrete structures, (2014).
[11] E. Standard, En 1992-1-1, (2004).
[12] B.B. Adhikary, H. Mutsuyoshi, Shear strengthening of RC beams with web-bonded continuous steel plates, Constr. Build. Mater. 20 (2006) 296–307, https://doi.org/10.1016/j.conbuildmat.2005.01.026.
[13] C.E. Chalioris, G.E. Thermou, S.J. Pantazopoulou, Behaviour of rehabilitated RC beams with self-compacting concrete jacketing - analytical model and test results, Constr. Build. Mater. 55 (2014) 257–273, https://doi.org/10.1016/J.CONBUILDMAT.2014.01.031.
[14] P. Colajanni, A. Recupero, N. Spinella, Increasing the shear capacity of reinforced concrete beams using pretensioned stainless steel ribbons, Struct. Concr. 18 (2017) 444–453, https://doi.org/10.1002/SUCO.201600089.
[15] P. Colajanni, A. Recupero, N. Spinella, Increasing the flexural capacity of RC beams using steel angles and pre-tensioned stainless steel ribbons, Struct. Concr. 17 (2016) 848–857, https://doi.org/10.1002/SUCO.201500187.
[16] R.M. Foster, C.T. Morley, J.M. Lees, Shear transfer across a diagonal crack in reinforced concrete strengthened with externally bonded FRP fabric, Advanced Composites in Construction 2013, ACIC 2013 - Conference Proceedings. (2013) 166–177.
[17] R. El-Hacha, K. Soudki, Prestressed near-surface mounted fibre reinforced polymer reinforcement for concrete structures - a review, Can. J. Civ. Eng. 40 (2013) 1127–1139, https://doi.org/10.1139/CJCE-2013-0063.

[18] P. Soroushian, K. Ostowari, A. Nossoni, H. Chowdhury, Repair and strengthening of concrete structures through application of corrective posttensioning forces with shape memory alloys, Transp. Res. Rec. 1770 (1) (2001) 20–26.
[19] L. Zerbe, M. Reda, M. Dawood, A. Belarbi, A. Senouci, B. Genckturk, M. Al-Ansari, J. Michel, in: Behavior of retrofitted concrete members using iron-based shape memory alloys, Fourth Conference on Smart Monitoring Assesment and Rehabilitation of Civil Structures, 2017, p. 9.
[20] L. Janke, C. Czaderski, M. Motavalli, J. Ruth, Applications of shape memory alloys in civil engineering structures—overview, limits and new ideas, Mat. Struct. 38 (5) (2005) 578–592.
[21] M.S. Alam, M.A. Youssef, M. Nehdi, Utilizing shape memory alloys to enhance the performance and safety of civil infrastructure: a review, Can. J. Civ. Eng. 34 (2007) 1075–1086, https://doi.org/10.1139/L07-038.
[22] A. Cladera, B. Weber, C. Leinenbach, C. Czaderski, M. Shahverdi, M. Motavalli, Iron-based shape memory alloys for civil engineering structures: an overview, Constr. Build. Mater. 63 (2014) 281–293, https://doi.org/10.1016/j.conbuildmat.2014.04.032.
[23] C. Czaderski, M. Shahverdi, R. Brönnimann, C. Leinenbach, M. Motavalli, Feasibility of iron-based shape memory alloy strips for prestressed strengthening of concrete structures, Constr. Build. Mater. 56 (2014) 94–105, https://doi.org/10.1016/j.conbuildmat.2014.01.069.
[24] S. Abouali, M. Shahverdi, M. Ghassemieh, M. Motavalli, Nonlinear simulation of reinforced concrete beams retrofitted by near-surface mounted iron-based shape memory alloys, Eng. Struct. 187 (2019) 133–148, https://doi.org/10.1016/J.ENGSTRUCT.2019.02.060.
[25] M. Shahverdi, C. Czaderski, M. Motavalli, Iron-based shape memory alloys for prestressed near-surface mounted strengthening of reinforced concrete beams, Constr. Build. Mater. 112 (2016) 28–38, https://doi.org/10.1016/J.CONBUILDMAT.2016.02.174.
[26] J. Michels, M. Shahverdi, C. Czaderski, Flexural strengthening of structural concrete with iron-based shape memory alloy strips, Struct. Concr. 19 (2018) 876–891, https://doi.org/10.1002/SUCO.201700120.
[27] K. Hong, S. Lee, Y. Yeon, K. Jung, Flexural response of reinforced concrete beams strengthened with near-surface-mounted fe-based shape-memory alloy strips, Int. J. Concr. Struct. Mater. 12 (2018) 1–13, https://doi.org/10.1186/S40069-018-0279-Y/FIGURES/13.
[28] H. Rojob, R. El-Hacha, Fatigue performance of RC beams strengthened with self-prestressed iron-based shape memory alloys, Eng. Struct. 168 (2018) 35–43, https://doi.org/10.1016/J.ENGSTRUCT.2018.04.042.
[29] M. Shahverdi, J. Michels, C. Czaderski, M. Motavalli, Iron-based shape memory alloy strips for strengthening RC members: material behavior and characterization, Constr. Build. Mater. 173 (2018) 586–599, https://doi.org/10.1016/j.conbuildmat.2018.04.057.
[30] A. Muntasir Billah, J. Rahman, Q. Zhang, Shape memory alloys (SMAs) for resilient bridges: A state-of-the-art review, Structures. 37 (2022) 514–527, https://doi.org/10.1016/J.ISTRUC.2022.01.034.
[31] C. Qiu, A. Zhang, T. Jiang, X. Du, Seismic performance analysis of multi-story steel frames equipped with FeSMA BRBs, Soil Dyn. Earthq. Eng. 161 (2022), 107392, https://doi.org/10.1016/J.SOILDYN.2022.107392.
[32] M.A. Molod, P. Spyridis, F.J. Barthold, Applications of shape memory alloys in structural engineering with a focus on concrete construction – a comprehensive review, Constr. Build. Mater. 337 (2022), 127565, https://doi.org/10.1016/J.CONBUILDMAT.2022.127565.
[33] G. Singh Rajput, J. Vora, P. Prajapati, R. Chaudhari, Areas of recent developments for shape memory alloy: a review, Mater. Today:. Proc. 62 (2022) 7194–7198.
[34] L.A. Montoya-Coronado, J.G. Ruiz-Pinilla, C. Ribas, A. Cladera, Experimental study on shear strengthening of shear critical RC beams using iron-based shape memory alloy strips, Eng. Struct. 200 (2019) 109680.
[35] W.C.K. Otsuka, Shape memory materials, Cambridge University Press, United Kingdom, 1998.
[36] J.G. Ruiz-Pinilla, L.A. Montoya-Coronado, C. Ribas, A. Cladera, Finite element modeling of RC beams externally strengthened with iron-based shape memory alloy (Fe-SMA) strips, including analytical stress-strain curves for Fe-SMA, Eng. Struct. 223 (2020), 111152, https://doi.org/10.1016/J.ENGSTRUCT.2020.111152.
[37] W. Ramberg, W.R. Osgood, Description of stress-strain curves by three parameters, National Advisory Committee For Aeronautics. (1943) Technical Note No. 902.
[38] M.J. Shahverdi M, Czaderski C, 'memory steel' for Shear Reinforcement of Concrete Structures, in: SMAR 2019- Fifth Conf. Smart Monit. Assess. Rehabil. Civ. Struct., Potsdam, 2019.
[39] A. Cladera, L.A. Montoya-Coronado, J.G. Ruiz-Pinilla, C. Ribas, Shear strengthening of slender reinforced concrete T-shaped beams using iron-based shape memory alloy strips, Eng. Struct. 221 (2020), 111018, https://doi.org/10.1016/J.ENGSTRUCT.2020.111018.
[40] A. Monserrat López, P.F. Miguel Sosa, J.L. Bonet Senach, M.Á. Fernández Prada, Influence of the plastic hinge rotations on shear strength in continuous reinforced concrete beams with shear reinforcement, Eng. Struct. 207 (2020), 110242, https://doi.org/10.1016/J.ENGSTRUCT.2020.110242.
[41] A. Monserrat López, P.F. Miguel Sosa, J.L. Bonet Senach, M.Á. Fernández Prada, Experimental study of shear strength in continuous reinforced concrete beams with and without shear reinforcement, Eng. Struct. 220 (2020), 110967, https://doi.org/10.1016/J.ENGSTRUCT.2020.110967.
[42] S.M. Lopes, R.N.F. do Carmo, Deformable strut and tie model for the calculation of the plastic rotation capacity, Comput. Struct. 84 (2006) 2174–2183, https://doi.org/10.1016/J.COMPSTRUC.2006.08.028.
[43] R. Vaz Rodrigues, A. Muttoni, M.F. Ruiz, Influence of shear on rotation capacity of reinforced concrete members without shear reinforcement, ACI Struct. J. 107 (2010) 516–525, https://doi.org/10.14359/51663902.
[44] J.M. Rius, A. Cladera, C. Ribas, B. Mas, Shear strengthening of reinforced concrete beams using shape memory alloys, Constr. Build. Mater. 200 (2019) 420–435, https://doi.org/10.1016/J.CONBUILDMAT.2018.12.104.
[45] K.K. Alaneme, E.A. Okotete, Reconciling viability and cost-effective shape memory alloy options – a review of copper and iron based shape memory metallic systems, Eng. Sci. Technol. An Int. J. 19 (2016) 1582–1592, https://doi.org/10.1016/j.jestch.2016.05.010.
[46] A. Monserrat López, M. Fernánez Ruiz, P.F. Miguel Sosa, The influence of transverse reinforcement and yielding of flexural reinforcement on the shear-transfer actions of RC members, Eng. Struct. 234 (2021), 111949, https://doi.org/10.1016/J.ENGSTRUCT.2021.111949.
[47] A. Muttoni, M.F. Ruiz, Shear strength of members without transverse reinforcement as function of critical shear crack width, ACI Struct. J. 105 (2008) 163–172, https://doi.org/10.14359/19731.
[48] A. Monserrat López, Comportamiento frente a cortante de vigas continuas de hormigón armado estudio experimental de los mecanismos resistentes y de la influencia de la cinemática desarrollada en combinación con los esfuerzos de flexión, 2020. https://dialnet.unirioja.es/servlet/tesis?codigo=293050.
[49] S. Campana, F.R. M, A. Anastasi, A. Muttoni, S. Campana, Analysis of shear-transfer actions on one-way RC members based on measured cracking pattern and failure kinematics, 56 (2013) 386–404.
[50] B. Mas, A. Cladera, C. Ribas, Experimental study on concrete beams reinforced with pseudoelastic Ni-Ti continuous rectangular spiral reinforcement failing in shear, Eng. Struct. 127 (2016) 759–768, https://doi.org/10.1016/J.ENGSTRUCT.2016.09.022.
[51] J.M. Rius, A. Cladera, B. Mas, C. Ribas, Shear behaviour of beams strengthened using different Ni-Ti-Nb shape memory alloy wire configurations and design proposal based on the compression chord Capacity model (CCCM), Eng. Struct. 268 (2022) 114724.
[52] re-fer AG, Product data sheet re-plate "for statically loaded members," (n.d.).